LA-8353-MS

Informal Report

c. 3

CIC-14 REPORT COLLECTION
REPRODUCTION
COPY

The Status of Monte Carlo at Los Alamos

LOS ALAMOS NATIONAL LABORATORY
3 9338 00313 5018

University of California

LOS ALAMOS SCIENTIFIC LABORATORY
Post Office Box 1663 Los Alamos, New Mexico 87545

An Affirmative Action/Equal Opportunity Employer

This report was not edited by the Technical Information staff.

This report was prepared as an account of work sponsored by the United States Government. Neither the United States nor the United States Department of Energy, nor any of their employees, makes any warranty, express or implied, or assumes any legal liability or responsibility for the accuracy, completeness, or usefulness of any information, apparatus, product, or process disclosed, or represents that its use would not infringe privately owned rights. Reference herein to any specific commercial product, process, or service by trade name, mark, manufacturer, or otherwise, does not necessarily constitute or imply its endorsement, recommendation, or favoring by the United States Government or any agency thereof. The views and opinions of authors expressed herein do not necessarily state or reflect those of the United States Government or any agency thereof.

UNITED STATES
DEPARTMENT OF ENERGY
CONTRACT W-7405-ENG. 36

LA-8353-MS
Informal Report

UC-20, UC-32, UC-80
Issued: May 1980

The Status of Monte Carlo at Los Alamos

W. L. Thompson
E. D. Cashwell
T. N. K. Godfrey
R. G. Schrandt
O. L. Deutsch
T. E. Booth

LOS ALAMOS NATL. LAB. LIBS.
3 9338 00313 5018

Foreword

The following four papers were presented by Group X-6 on April 22, 1980, at the Oak Ridge Radiation Shielding Information Center (RSIC) Seminar-Workshop on Theory and Applications of Monte Carlo Methods.

These papers are combined into this one report for convenience and because they are related to each other. The first paper (by Thompson and Cashwell) is a general survey about X-6 and MCNP and is an introduction to the other three papers. It can also serve as a resume' of X-6. The second paper (by Godfrey) explains some of the details of geometry specification in MCNP. The third paper (by Cashwell and Schrandt) illustrates calculating flux at a point with MCNP; in particular, the once-more-collided flux estimator is demonstrated. Finally, the fourth paper (by Thompson, Deutsch, and Booth) is a tutorial on some variance-reduction techniques. It should be required reading for a fledging Monte Carlo practitioner.

Members of Group X-6 include: T. E. Booth, J. F. Briesmeister, E. D. Cashwell, J. B. Coleman, O. L. Deutsch, J. J. Devaney, G. P. Estes, C. J. Everett, J. C. Ferguson, R. A. Forster, T. N. K. Godfrey, J. S. Hendricks, R. J. Juzaitis, R. C. Little, D. M. Morris, R. E. Prael, R. G. Schrandt, R. E. Seamon, P. D. Soran, W. M. Taylor, W. L. Thompson, and J. K. Treadaway.

W. L. Thompson
X-6 Group Leader

CONTENTS

		Page
I.	The Status of Monte Carlo at Los Alamos (W. L. Thompson and E. D. Cashwell)	1
II.	Geometry in MCNP (T. N. K. Godfrey)	17
III.	Flux at a Point in MCNP (E. D. Cashwell and R. G. Schrandt)	23
IV.	Deep-Penetration Calculations (W. L. Thompson, O. L. Deutsch and T. E. Booth)	36

THE STATUS OF MONTE CARLO AT LOS ALAMOS

by

W. L. Thompson, E. D. Cashwell, T. N. K. Godfrey,
R. G. Schrandt, O. L. Deutsch, T. E. Booth

ABSTRACT

This report is a compilation of four papers presented at the 1980 Radiation Shielding Information Center Monte Carlo Seminar in Oak Ridge. The papers describe the Los Alamos Scientific Laboratory Monte Carlo group (X-6), its code MCNP, and some applications of MCNP.

THE STATUS OF MONTE CARLO AT LOS ALAMOS

William L. Thompson and Edmond D. Cashwell
Group X-6
Monte Carlo, Applications, and Transport Data Group
Theoretical Applications Division
Los Alamos Scientific Laboratory
Los Alamos, New Mexico 87545

ABSTRACT

At Los Alamos the early work of Fermi, von Neumann, and Ulam has been developed and supplemented by many followers, notably Cashwell and Everett; and the main product today is the continuous-energy, general-purpose, generalized-geometry, time-dependent, coupled neutron-photon transport code called MCNP. The Los Alamos Monte Carlo research and development effort is concentrated in Group X-6.

MCNP treats an arbitrary three-dimensional configuration of arbitrary materials in geometric cells bounded by first- and second-degree surfaces and some fourth-degree surfaces (elliptical tori). MCNP has its own cross-section libraries plus it allows two thermal neutron models: the free-gas and $S(\alpha,\beta)$ treatments. There is a wide variety of standard sources plus a very easy-to-use and extensive tally structure. MCNP is quite rich in variance-reduction schemes, including three different techniques for estimating flux at a point. Other features include being able to calculate eigenvalues for both sub- and super-critical systems, an elaborate plotter for checking geometry setups, calculation of cell volumes and surface areas, and good documentation.

Monte Carlo has evolved into perhaps the main method for radiation transport calculations at Los Alamos. MCNP is used in every technical division at the Laboratory by over 130 users about 600 times a month accounting for nearly 200 hours of CDC-7600 time. However, MCNP is just the parent code. In addition to MCNP, major variants supported by Group X-6 include a multigroup forward and adjoint code, a code allowing geometrical perturbations, and a code that allows cell boundaries to change as a function of time. In addition, Group X-6 is involved in electron and high-energy nucleon/meson transport by Monte Carlo.

INTRODUCTION

We are happy to report that Monte Carlo is alive and well at Los Alamos. Our main code, MCNP,[1] is used by about 130 users in virtually every technical division at the Laboratory over 600 times a month, accounting for nearly 200 hours of CDC-7600 computer time. Monte Carlo, and in particular MCNP, is possibly the main method for radiation transport calculations at Los Alamos today. MCNP is also actively supported by Group X-6 on the Magnetic Fusion Energy computer network where it is used by a number of people throughout the country. Although Monte Carlo has widespread use at Los Alamos, the main research, code development and maintenance, user support, documentation, and nonroutine applications are concentrated in Group X-6 in the Theoretical Applications Division (X-Division). The purpose of this paper is to tell you a little about X-6 and its codes, with emphasis on MCNP.

GROUP X-6

Group X-6, presently consisting of 22 members, has as its title "Monte Carlo, Applications, and Transport Data." From this title, it is clear we have three areas of concern: (1) Monte Carlo methods and code development, (2) applications requiring particle transport by Monte Carlo, and (3) cross-section data. A strength of the group lies in the interaction of these three areas and their support of one another. To a very large extent, all the people in X-6 are conversant in each of these areas and appreciate the requirements and problems of each. The magnitude of the Monte Carlo expertise that resides in X-6 is likely unrivaled.

Activities in each of these areas will be discussed, but to help clarify the role of Group X-6 relative to some other activities at Los Alamos that you may be familiar with, the role of two groups from the Theoretical Division will be briefly mentioned. Group T-1, headed by D. J. Dudziak, is where the Laboratory's S_n expertise is concentrated. They are responsible for codes like ONETRAN[2] and TRIDENT.[3] Like X-6 they also are involved in applications but specialize in S_n and occasionally use the X-6 Monte Carlo codes as we in X-6 occasionally use their S_n codes. Basically though, we in X-6 solve transport problems randomly and T-1 solves transport problems discretely. Group T-2, headed by P. G. Young, is the Laboratory's nuclear data group. Among other activities, T-2 evaluates cross sections and processes data sets with their codes such as NJOY;[4] X-6 does not evaluate cross sections but extensively tests them and then makes them available in proper form for direct use by many of the major transport codes at LASL.

Monte Carlo Methods and Code Development

X-6 responds to requests from throughout the Laboratory for new methods and techniques to help solve individual problems. The requests are

frequently very specific and limited in scope (such as how to sample from some exotic distribution), but the requests may lead to a new feature that becomes a permanent part of our codes. Furthermore, X-6 originates many new methods and code improvements based on its knowledge of Monte Carlo and applications.

Some of the recent accomplishments include an $S(\alpha,\beta)$ thermal treatment, a more general analytical volume and surface-area calculator,[5] a very general tally structure, a once-more-collided point detector routine with a bounded variance, the addition of the union and complement operators for geometry specification, new standard sources with improved directional biasing into a fixed cone or in a continuous manner by means of an exponential function, a way to deterministically transport particles during their random walk (DXTRAN), many more user-oriented features and safeguards, plus a long list of miscellaneous items. A major accomplishment has been in the area of code documentation with the publishing of the 411-page MCNP manual[1] that contains over a hundred pages each of theory, cookbook examples, and details of the coding.

In the area of Monte Carlo theory, the theory of errors is a significant topic in X-6,[6-9] and a major work on relativistic effects has just been published.[10]

A new area of code development and physics for X-6 is the transport of high-energy (GeV range) protons, pions, mesons and the complete cascade of secondary particles down to the thermal-energy range. Applications will include energy deposition calculations in tissue in conjunction with the Los Alamos Meson Physics Facility research in cancer treatment plus shielding and materials damage studies. Our work is based on a modification to the HETC[11] code with an interface to MCNP.

In addition to the parent code MCNP, other X-6 codes include MCMG[12] which is a multigroup version of MCNP that also has an adjoint capability, MCNPPER that allows geometrical perturbations for calculating derivative information, MCGE which is a coupled electron-photon code that addresses the complete electron-photon cascade in the energy range from 20 MeV to 100 keV, a code that allows geometrical boundaries to change as a function of time, and numerous special versions of MCNP with which we evaluate new techniques and solve specialized problems.

About 40% of our effort is spent in this area.

Applications

X-6 serves two roles in the area of applications: (1) we work closely with MCNP users to help them with their applications, and (2) we do many applications ourselves that require our expertise and experience. Both these roles are valuable because they give us feedback on the use of MCNP and how best to improve it, and they broaden our own experience with a variety of applications.

Many applications are related to data verification and will be mentioned in that context.

An ongoing responsibility that we have for the Laboratory is calculating the biological dose from the intrinsic radiation (from the various natural decay modes of plutonium and uranium isotopes) emitted from the nuclear material used in nuclear weapons. This is of concern when military personnel are required to be in the proximity of the weapons for extended periods of time as is the case on a submarine. We also perform many calculations related to the vulnerability and effects of nuclear weapons.

X-6 has done extensive neutronics calculations for magnetic fusion reactor designs such as the Elmo Bumpy Torus (EBT),[13] Linus,[14] Reversed Field Pinch Reactor (RFPR)[15] and Fast-Liner Reactor[16] concepts. Furthermore, studies were made on Tokamak designs to evaluate the effect of geometrical simplifications in calculations.[17] Figure 1 is a Tokamak reactor geometry set up for MCNP; the surfaces marked by asterisks are tori. We would like to increase our role in the magnetic fusion area.

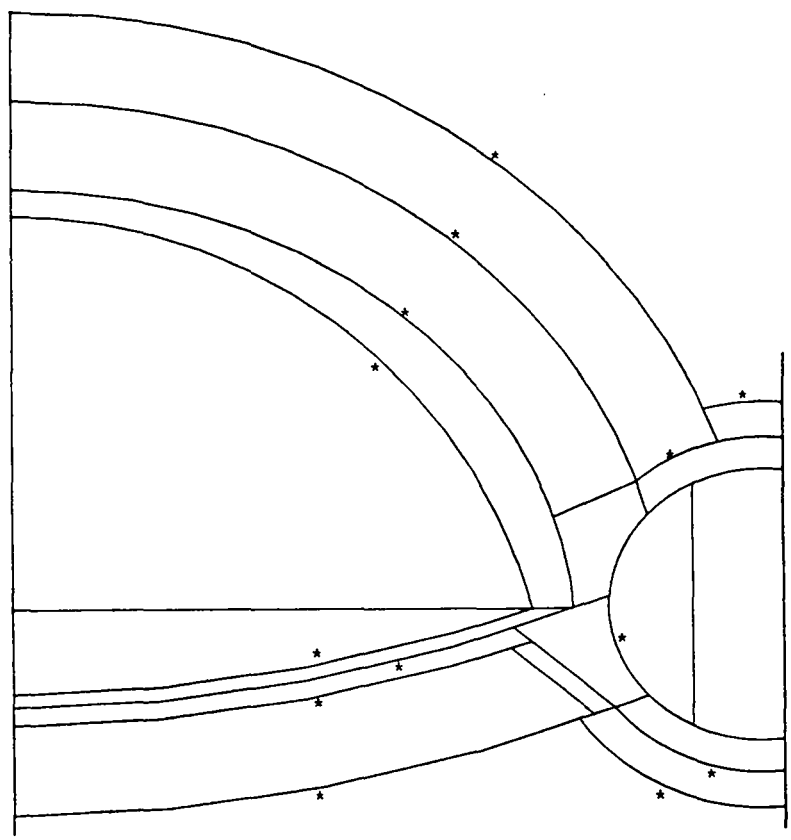

Figure 1. Tokamak Geometry.

The shielding designs for new facilities to be built at Los Alamos are frequently done by X-6. Recent examples include shielding from bremsstrahlung for a new electron accelerator to be built by the Physics Division and for the Antares Laser Fusion facility being built by the Laser Division. The Monte Carlo bulk-shielding calculations were done for Antares during the early design of the facility.[18] The basic building has been constructed, and we are now doing a radiation mapping inside the Target Building to ascertain material and instrumentation damage plus activation analysis of the target-chamber components. Figure 2 is the MCNP representation of the Antares target-insertion mechanism.

An activation analysis code, using the LASL GAMMON library,[19] is coupled with MCNP and calculates gas production (H,D,T, and He), material activation, and photon sources. The photon sources can be used in MCNP to calculate dose rates at points of interest.

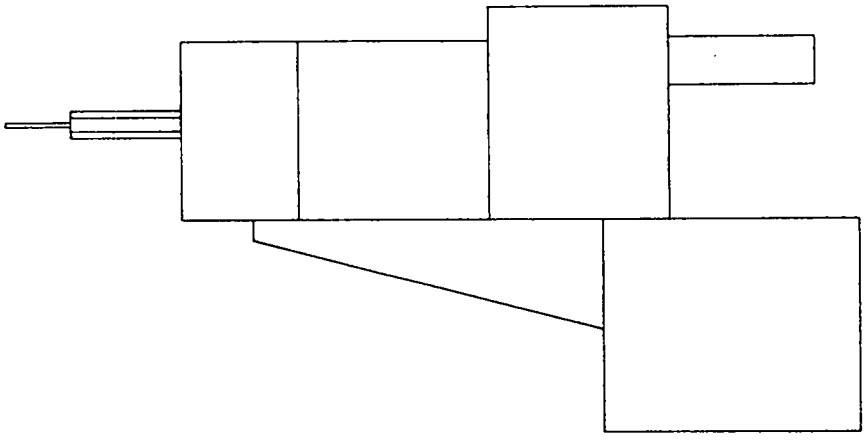

Figure 2. Antares Target-Insertion Mechanism.

Many interesting calculations have been done for the Health Division that involve instrument design[20,21] and radiation safety. One project involved the design of the gloveboxes at the new Plutonium Facility at Los Alamos, and another project just completed was a criticality study for the Slagging Pyrolysis Incinerator Facility (SPI) to be built at Idaho Falls.[22]

A recent series of calculations was completed as part of the review of the design of the Fusion Material Irradiation Test Facility (FMIT) to be built at Hanford.

X-6 works closely with the Nuclear Safeguards (assay and accountability) groups at Los Alamos in the designing of instrumentation, helping to understand the physics and Monte Carlo simulation of their experiments, and providing special versions of MCNP to account for delayed neutrons and to simulate coincidence counters.[23] Calculations in this area are invaluable to optimize an instrument design and to understand or extrapolate a calibration curve in the assay of unknowns.

About 35% of X-6's effort is spent in the area of applications.

Transport Data

X-6 is responsible for the X-Division nuclear cross sections and does partial processing of cross-section data provided by Group T-2. This includes continuous-energy, multigroup, and radiochemistry data used not only in the X-6 Monte Carlo codes but also in other transport codes used in X-Division and throughout the Laboratory.

The major effort in this third area of X-6 work is the testing of cross-section data.[24] The data are verified by two methods: (1) differential testing involving spectra, and (2) integral testing involving critical mass calculations of Los Alamos assemblies like Godiva and Jezebel. As part of this cross-section work, X-6 has been calculating and analyzing the latest experiment designed to measure the neutron spectrum and tritium production, and to check specific cross sections at various locations in a system consisting of a 93.5% enriched uranium sphere surrounded by ^{6}LiD. The Livermore pulsed-sphere experiments are also calculated for integral testing of cross-section data.

Extensive thermal benchmark calculations have recently been completed to test the integrity of MCNP, its thermal treatments, and its data.[25] MCNP calculations are now making significant contributions to the thermal data-testing program.

We have recently completed the monumental task of thinning, testing, and assembling in suitable form the ENDF/B-V and Livermore ENDL79 data. These data are now being used at Los Alamos.[26-28]

This final area accounts for about 25% of the group's effort. We find having this cross-section effort an integral part of X-6 to be a very valuable arrangement. It gives those of us doing applications a greater appreciation and awareness of the data. Furthermore, great resources can be immediately brought to bear on questions of transport data - as illustrated in the following paper on deep-penetration calculations by Thompson, Deutsch, and Booth.

As mentioned earlier, Group X-6 is the author of MCNP, and MCNP is the backbone and main product of X-6.

MCNP is a very mature and reliable Monte Carlo code. It represents over two hundred man-years of effort and is the culmination of the original Monte Carlo work at Los Alamos by Fermi, von Neumann, and Ulam. Cashwell and Everett, over a period of almost thirty years, have contributed most to the development of MCNP. The first book on Monte Carlo was written by Cashwell and Everett.[29]

MCNP is a general-purpose, continuous-energy, generalized-geometry, time-dependent, coupled neutron-photon Monte Carlo transport code. It may be used in any of three modes: (1) neutron transport only, (2) combined neutron-photon transport, or (3) photon transport only. The capability to calculate eigenvalues for critical systems is also a standard feature of MCNP.

The following few sections will point out the main features of MCNP but will not go into detail. The MCNP manual, in addition to explaining how to use the code, contains the details of the physics, mathematics, and nuclear data aspects of MCNP. Another short publication,[30] which is just a reprint of the first part of the manual, summarizes the code. Finally, Carter and Cashwell's book[31] is not only a good general reference on radiation transport by Monte Carlo, but it is based upon MCNP in many aspects.

For most applications of MCNP, the user has to supply no more than an input file describing a problem. All of the input to MCNP is in free format. There is a variety of standard sources to choose from, and the tally structure is very general and elaborate. There is no need for a user to compile cross-section libraries for problems; X-6 maintains and provides all the data needed by MCNP.

Nuclear Data and Reactions

MCNP is a continuous-energy Monte Carlo code that makes no gross approximations regarding data. Linear interpolation is used between energy points with a few hundred to several thousand points typically required to reproduce the original data within a specified tolerance (in fact, usually within 0.1 to 0.5%). The only significant difference between the MCNP data libraries and the ENDF/B library (from which it is derived with the NJOY processing code) is that resonance data are represented in MCNP as linearly interpolated pointwise data that are Doppler broadened to a specific temperature. All reactions given in a particular neutron cross-section evaluation are accounted for in the energy range from 20 MeV to 10^{-5} eV. Users can choose from data with prompt or total fission ν's as well as

having the option to use a set of discrete-reaction cross sections in which the reaction cross sections have been collapsed into 240 energy groups to save computer memory. Users have the choice of data from the ENDF/B, British AWRE, Livermore ENDL, or special LASL libraries.

There are two thermal treatments in MCNP. One is the free-gas model in which, for elastic collisions, light atoms (Z = 1 through 8) are assumed to be in a Maxwellian distribution with some thermal temperature that may be a function of time. Secondly, the $S(\alpha,\beta)$ scattering model is available which accounts for chemical binding and crystalline effects at very low energies. Typically, when going down to room temperature, the free-gas model is used from around 10 eV to 4 eV, and then the $S(\alpha,\beta)$ model is used below that.

Photon interactions are accounted for in the range of 100 MeV to 1 keV. MCNP accounts for both incoherent and coherent scattering, fluorescent emission following photoelectric absorption, and pair production.

Geometry

The geometry of MCNP treats a general three-dimensional configuration of arbitrarily-defined materials in geometric cells bounded by first- and second-degree surfaces and some special fourth-degree surfaces (elliptical tori). The cells are defined by the intersections, unions, and complements of regions bounded by the surfaces.

Surfaces are easily defined by supplying coefficients to the analytic surface equations or by indicating known points located on the surfaces. For example, the surface $y - D = 0$ is represented in MCNP by the mnemonic PY with the single entry D. Therefore, a plane normal to the y-axis at $y = 4$ is defined by the simple input line of

```
PY    4
```

MCNP has 26 such mnemonics available.

Figure 3 is a geometry set up to test the analytical volume calculator in MCNP (the volume was calculated analytically and also stochastically by using a track-length estimator). This geometry of a fancy fish with a weird sun is actually only three cells in the MCNP problem: (1) the disjoint regions of the fish plus the sun (which appears as four regions), (2) everything else inside the sphere, and (3) everything outside the sphere. The geometry was specified by portions of twenty-three surfaces consisting of six tori, two hyperboloids, two ellipsoids, seven cones, one cylinder, two spheres, and three planes.

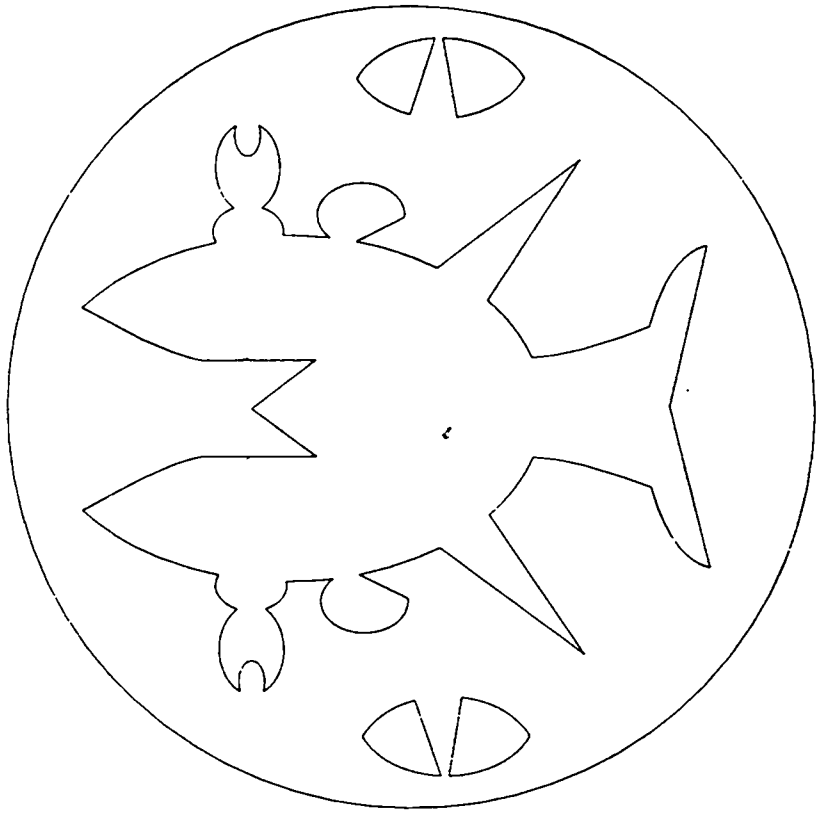

Figure 3. Example of MCNP Geometry.

Figure 4 is another example of MCNP geometry. This geometry consists of two cells and fifteen surfaces. The numbers in the figure refer to surface numbers: surface 1 is a cylinder; 3 is a cone; 12 and 13 are planes; 6, 7, 14 and 15 are ellipsoids; and 2, 5, 9, 10, and 11 are planes of two sheets.

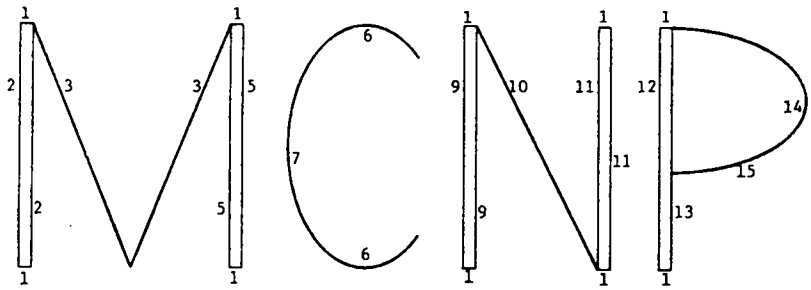

Figure 4. Example of MCNP Geometry.

More details about the MCNP geometry are given in the following paper by Godfrey. The significant additions of the union and complement operators to our geometry vocabulary are products of Godfrey's work. Cells that are now routinely specified with the union operator that are illegitimate when using intersections only are now in fact called "Godfrey cells" by us.

Variance Reduction

This one area alone makes MCNP a superb Monte Carlo code; MCNP is rich in variance-reduction techniques. The following two papers by Cashwell and Schrandt and by Thompson, Deutsch, and Booth will illustrate some of these techniques. More details are available in Refs. 1 and 31.

In addition to obvious ways to save computer time like using energy and time cutoffs, MCNP offers geometry splitting with Russian roulette, analog capture or survival biasing with weight cutoff and Russian roulette, correlated sampling, the exponential transformation, energy splitting, forced collisions, flux estimates at points by three methods (next-event estimator, ring detector, and once-more-collided estimator), track-length estimators, source biasing in direction and energy, and a combination random walk/deterministic scheme called DXTRAN. Furthermore, a Russian roulette game can be played with detector or DXTRAN contributions as a function of mean free path that can save substantial computer time.

X-6 is always evaluating new variance-reduction techniques and improving existing ones. Examples are (1) angle biasing which we look at from time to time but to date have not found a scheme that has anything substantial to offer over other methods already in MCNP, and (2) a weight window that looks quite promising (see paper by Thompson, Deutsch, and Booth). Furthermore, we are looking at generalized phase-space splitting.

Tallies

An important part of the MCNP output that the user has little control over (except for all of it or a fixed subset of it) is summary and diagnostic information. This information is valuable for determining the characteristics of a problem and the effect of variance-reduction techniques. Examples are (1) a complete breakdown of all energy and weight creation and loss mechanisms averaged over the entire problem and also individually by cell, (2) the number of tracks entering a cell and the track population in a cell, (3) the average energy, weight, number of collisions, and mean free path in a cell, (4) the volume, mass, and surface area of a cell, and (5) the activity (i.e., collisions, collisions times weight, and weight lost to capture) of each nuclide in each cell.

In addition to this summary information, MCNP has an elaborate and easy-to-use tally structure that allows the user to tally almost anything conceivable. Choices include, as a function of energy and time,

(1) current as a function of direction across a surface, (2) flux across a surface, (3) flux at a point, (4) average flux in a cell, and (5) energy deposition (or heating) in a cell by neutrons, photons, and products of neutron reactions. Surfaces or cells may be subdivided into segments for tallying purposes. In addition, particles may be flagged when they cross specified surfaces or enter designated cells, and the contributions of these flagged particles to the tallies are listed separately. The user has available a special subroutine by which the standard tallies can be modified in almost any desired way.

Reactions such as fission, absorption, tritium production, or any product of the flux times the approximately one hundred standard ENDF/B reactions plus several nonstandard ones may be tallied very simply.

Printed out with each tally is also its estimated relative error corresponding to one standard deviation of the mean.

Other Features

MCNP has the capability to calculate eigenvalues for critical systems. Three estimators (in various combinations) are used to calculate k_{eff}: absorption, collision, and track-length estimators.

For debugging input and geometries, MCNP makes extensive and elaborate checks for consistency. A plotting capability is in MCNP that provides an arbitrary cross-sectional view of the input geometry on several output devices (all figures in this paper plus slides used in the oral presentation were generated by the plotter). If a track gets lost during its transport, diagnostics are automatically printed for that track which include an event log. The event log is a print of the complete life of the track from event to event (birth, collisions, surface crossing, etc.).

A feature is available to allow the user to translate and/or rotate surfaces from one coordinate system to another. For example, it is a nontrivial task to determine the coefficients for the general quadratic equation needed to define an ellipse with its origin off somewhere in space and its axes at some skewed angle. However, an ellipse can be easily defined centered about the coordinate-system origin with axes parallel to the coordinate axes. It is then an easy procedure to move the simple ellipse to another place with another orientation.

For tallying purposes, cell volumes and surface areas are analytically calculated for polyhedral cells and for any cell bounded by surfaces of revolution (regardless of axis of symmetry). Surfaces of revolution generally account for the majority of cells, but irregular volumes and surface areas can also be easily calculated stochastically.

A convenient mechanism is provided to specify information to be written to a file for post-processing, such as for plotting results or to generate a source for a subsequent problem.

Full restart capabilities are available that are used for machine failure or continuing a run to obtain better statistics.

Future Work

We are the first to recognize that MCNP does not do everything for everybody. We are cautious about what goes into the code and put something in only for a good reason and after it has been carefully evaluated. However, X-6 frequently creates special versions of MCNP for the one-time requirements of special calculations or for the special requirements of a limited number of users.

The two most obvious shortcomings for use outside of Los Alamos are a lattice geometry specification and a better treatment of unresolved resonances. The lattice capability has not been of overriding importance to us at Los Alamos, but if others are interested in this feature we could be persuaded to increase the priority of it.

As mentioned earlier, we are always improving the existing variance-reduction techniques and devising new ones. We are interested in photo-neutron transport, but this is mainly a problem of data. Work is presently in progress on a three-dimensional plotter; our geometries have become so complicated it is hard to comprehend them with two-dimensional slices. Graphical techniques are being explored for post-processing of output data and for visual aids to help understand the characteristics of a problem (i.e., where are the particles going and how does a variance-reduction technique influence them). Studies of Monte Carlo vectorization are underway to see how we can take advantage of modern computer architecture (such as the CRAY-1) or future computers with parallel, independent processors.

MCNP is not a static code. It is under constant scrutiny and development by X-6. We release a new version about once a year with the current code being Version 2A. If MCNP ever becomes static, it will be so because there is no further use for it. We do not anticipate this happening; rather, the opposite seems to be the case.

MCMG

The multigroup code MCMG has basically the same features as the continuous-energy code MCNP, but it relies on the same user-supplied multigroup, multitable cross-section data that are used in discrete ordinates codes. Unlike the data for MCNP, the multigroup data treatment results in problem-dependent cross sections that can place a burden on the user to assemble and understand. MCMG can be applied to standard shielding

problems, to problems in reactor physics including the use of thermal upscatter matrices, to problems in accelerator or cosmic-ray shielding at very high energies, to problems in neutral atom transport in plasmas, and to any other problem in linear transport for which multigroup data have been developed.

An added feature of MCMG is that it is also an adjoint code. A cell- and energy-dependent scalar flux is automatically generated during a forward-mode calculation, and this information is used for importance sampling of adjoint collisions and for an energy-dependent geometric splitting and Russian roulette game in the adjoint tracking.

The distribution of scattering angles for group-to-group transfer is represented by either continuous, equiprobable cosine bins or by MORSE-type discrete-scattering angles, both of which preserve all of the moments of the truncated Legendre representation.

MCMG has an advantage over discrete ordinates codes in that it does not suffer from geometrical restrictions. Like discrete ordinates codes, however, it can be limited by the approximations that are inherent in the multigroup data that can, for example, result in masking the existence of self-shielding effects.

CONCLUSION

In our opinion (admittedly biased in the true nature of Monte Carlo), Group X-6 is a very strong, experienced, and versatile Monte Carlo group. Our code MCNP is a leading Monte Carlo code because of its maturity, generality, ease of use, reliability, richness of variance-reduction techniques, documentation, cross-section libraries, and active support and development by the expertise of X-6.

REFERENCES

1. LASL Group X-6, "MCNP - A General Monte Carlo Code for Neutron and Photon Transport," LA-7396-M, Revised (November 1979).

2. T.R. Hill, "ONETRAN, A Discrete Ordinates Finite Element Code for the Solution of the One-Dimensional Multigroup Transport Equation," LA-5990-MS (June 1975).

3. T.J. Seed, "TRIDENT-CTR User's Manual," LA-7835-M (May 1979).

4. R.E. MacFarlane, R.J. Barrett, D.W. Muir, and R.M. Boicourt, "The NJOY Nuclear Data Processing System: User's Manual," LA-7584-M (December 1978).

5. J.S. Hendricks, "Calculation of Cell Volumes and Surface Areas in MCNP," LA-8113-MS (January 1980).

6. R.J. Juzaitis and T.E. Booth, "Minimizing Splitting Costs in Monte Carlo Particle Transport," Transactions of the ANS, 33, 713 (1979).

7. T.E. Booth and E.D. Cashwell, "Prediction of Computing Costs in Monte Carlo Transport Calculations," Transactions of the ANS, 33, 321 (1979).

8. C.J. Everett and E.D. Cashwell, "Cost of Splitting in Monte Carlo Transport," LA-7189-MS (March 1978).

9. T.E. Booth and E.D. Cashwell, "Analysis of Error in Monte Carlo Transport Calculations," Nuclear Science and Engineering, 71, 128 (1979).

10. C.J. Everett and E.D. Cashwell, "A Relativity Primer for Particle Transport, A LASL Monograph," LA-7792-MS (April 1979).

11. K.C. Chandler and T.W. Armstrong, "Operating Instructions for the High-Energy Nucleon-Meson Transport Code HETC," ORNL-4744 (January 1972).

12. O.L. Deutsch, "MCMG User's Guide," Internal X-6 Document (March 1979).

13. R.A. Krakowski and C.J. Bathke, "Reassessment of the Elmo Bumpy Torus Fusion Reactor Concept: Phase I, Physics Design," (P.D. Soran, Neutronics Design), LASL report in preparation.

14. R.W. Miller and R.A. Krakowski, "Reassesment of the Slowly-Imploding Liner (Linus) Fusion Reactor Concept," (P.D. Soran, Neutronics Design), LASL report in preparation.

15. R.L. Hagenson, R.A. Krakowski, G.E. Cort, "The Reversed-Field Pinch Reactor (RFPR) Concept," (P.D. Soran, Neutronics Design) LASL report LA-7973-MS (August 1979).

16. R.W. Moses, R.A. Krakowski and R.L. Miller, "A Conceptual Design of the Fast-Liner Reactor (FLR) for Fusion Power," (P.D. Soran, Neutronics Design), LASL report LA-7686-MS (February 1979).

17. J.L. Macdonald, E.D. Cashwell, and C.J. Everett, "Calculation of Toroidal Fusion Reactor Blankets by Monte Carlo," Proceedings of the Fifth International Conference on Reactor Shielding, Science Press, Princeton, 622 (1977).

18. W.L. Thompson, "A Neutron/Photon/Electron Shielding Study for a Laser Fusion Facility," Proceedings of the Fifth International Conference on Reactor Shielding, Science Press, Princeton, 628 (1977).

19. M.E. Battat, R.J. LaBauve, and D.W. Muir, "The GAMMON Activation Library," LA-8040-MS (September 1979).

20. D.A. Close and T.E. Booth, "In Situ Nondestructive Plutonium Assay for an Electropolishing Bath," Transactions of the ANS, 33, 423 (1979).

21. J.S. Hendricks and D.A. Close, "^{3}He Detector Design for Low-Level Transuranic Waste Assay," Transactions of the ANS, 28, 137 (1978).

22. D.A. Close, T.E. Booth, J.T. Caldwell, "Criticality Calculations and Criticality Monitoring Studies of the Slagging Pyrolysis Incinerator Facility," LA-8336-MS (April 1980).

23. J.E. Stewart, N. Ensslin, R.G. Schrandt, "Removing Multiplication Effects from Neutron Coincidence Counting Using Monte Carlo," Transactions of the ANS, 33, 442 (1979).

24. R.E. Seamon, "Cross Sections for Monte Carlo Calculations," X-6 Activity Report, LA-8232-PR, 34 (July-December, 1979).

25. R.E. Prael, "Thermal Reactor Benchmark Calculations with the MCNP Monte Carlo Code," Transactions of the ANS, 33, 846 (1979).

26. P.D. Soran and R.E. Seamon, "Integral Data Checking of ENDF/B-V and ENDL79," Internal X-6 memo (March 18, 1980).

27. G.P. Estes and J.S. Hendricks, "Integral Testing of Some ENDF/B-V Cross Sections," Transactions of the ANS, 33, 679 (November, 1979).

28. L.L. Carter and J.S. Hendricks, "Computational Benchmark for Deep Penetration in Iron," Transactions of the ANS, 33, 663 (1979).

29. E.D. Cashwell and C.J. Everett, "A Practical Manual on the Monte Carlo Method for Random Walk Problems," Pergamon Press, Inc., New York (1959), also LA-2120 (1957).

30. W.L. Thompson, "MCNP - A General Monte Carlo Code for Neutron and Photon Transport, A Summary," LA-8176-MS (December 1979).

31. L.L. Carter and E.D. Cashwell, "Particle-Transport Simulation with the Monte Carlo Method," ERDA Critical Review Series, TID-26607 (1975).

GEOMETRY IN MCNP

Thomas N.K. Godfrey
Group X-6
Monte Carlo, Applications and Transport Data Group
Los Alamos Scientific Laboratory
Los Alamos, New Mexico, USA

ABSTRACT

MCNP is a general-purpose neutron and photon Monte Carlo code developed by group X-6 at LASL. The geometry cells in MCNP are defined as regions of space bounded by user-specified second-degree surfaces and certain tori. Until recently cells had to have only convex edges. Now the geometry description is entirely general: cells may have concave edges and any sort of connectivity. The new general geometry description is a substantial improvement over the surface list and combinatorial geometry methods and includes the best features of both. It makes a big difference in the ease of setting up problems that contain features such as nested boxes, rooms with ells, and irregular slabs.

Another recent addition to the geometry description capability of MCNP is that certain kinds of surfaces of revolution can be defined by a few points on the surface rather than by the coefficients of the equation of the surface.

MCNP has long automatically calculated the volumes of rotationally symmetric cells. It now also calculates the volumes of polyhedral cells.

I will start with an example of how geometry is described in the setup of a problem for MCNP. I will then explain the vocabulary and syntax of the setup and show how tracking is done in the code. Finally, I will describe some of the other geometry features of MCNP and our plans for future improvements.

EXAMPLE OF GEOMETRY DESCRIPTION

In Fig. 1, cell 1 is a room with thick walls. The walls, including the columns, are collectively cell 2. There are other cells in the system that are not shown in the figure. The origin of coordinates is inside the

lower left column. The background grid consists of 1-meter squares. The portions of the problem input file for MCNP that describe cells 1 and 2 are shown in Table 1.

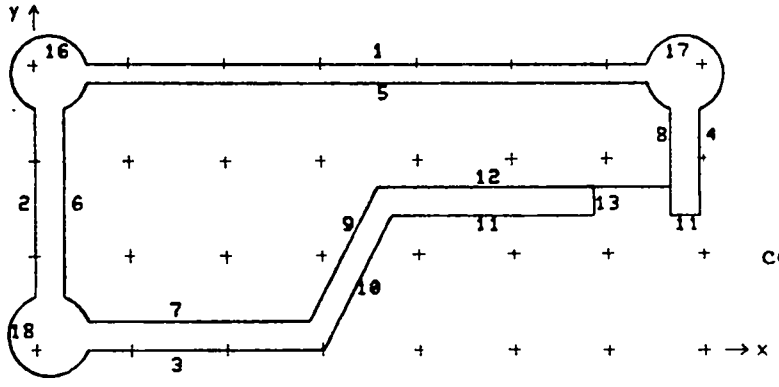

floor: surface 14
ceiling: surface 15

Fig. 1. Example of MCNP Geometry.

Table 1. Input File for Geometry of Fig. 1

```
cells
1     6 -5 -8 7 (12:-9) 16 17 18 14 -15
2     (2 -1 -4 3 :-16:-17:-18) #1 #(13 -12 -8) #(-11 10) 14 -15

surfaces
1     PY 300
2     PX 0
3     PY 0
4     PX 690
5     PY 280
6     PX 30
7     PY 30
8     PX 660
9     P 2 -1 0 540
10    P 2 -1 0 600
11    PY 140
12    PY 170
13    PX 580
14    PZ 0
15    PZ 310
16    C/Z 15 290 40
17    C/Z 675 290 40
18    C/Z 15 15 42.7
```

Each surface in the system is assigned a number. The specification of each surface is written on the line after the surface number. The specification of a surface consists of a symbol for the kind of surface

followed by the coefficients for the surface. For example, surface 1 is specified to be a plane perpendicular to the Y-axis (PY) at Y=300 cm. Surface 9 is a plane satisfying the equation

$$E(X,Y,Z) = Ax + By + Cz - D = 0$$
$$\text{with } A = 2,\ B = -1,\ C = 0, \text{ and } D = 540. \qquad (1)$$

Every point in space has a positive or negative sense with respect to each surface, unless it is actually someplace on the surface. The sense arises from the way the surfaces are required to be specified. Each kind of surface is described by an equation which is built into the code,

$$E(X,Y,Z) = 0. \qquad (2)$$

All points (X,Y,Z) for which the expression E(X,Y,Z) is greater than zero have a positive sense with respect to that surface. For example, the equation of surface 4 is

$$E(X,Y,Z) = X - D = 0 \quad \text{where } D = 690. \qquad (3)$$

So points to the right (large X) of surface 4 are positive with respect to surface 4, and points to the left of the surface are negative.

Cell 1 is specified as consisting of the intersection of the spaces to the right of surface 6, below surface 5, to the left of surface 8, above surface 7, and either above surface 12 or above and to the left of surface 9. The spaces where the columns encroach are excluded, and the cell is further limited by the floor and ceiling, surfaces 14 and 15. Cell 2 is the space enclosed by surfaces 2, 1, 4 and 3, plus the three columns, but excluding cell 1 and excluding the space enclosed by surfaces 13, 12, and 8. The space below surface 11 and to the right of surface 10 is excluded, and it is limited by the floor and ceiling.

VOCABULARY AND SYNTAX

The scheme used here is the combinatorial geometry of regions which are defined by simple surfaces. The regions are in most cases infinite, but in combination they define finite cells. The union operator is represented by the colon, the intersection operator is implicit, and the complement operator is represented by #. Where the complement operator is followed immediately by a number, the number is interpreted as a cell number. Otherwise all of the numbers are surface numbers. The region of space whose points have positive sense with respect to a surface is represented by the surface number. The region on the negative side is represented by the negative of the surface number. Parentheses are used

where necessary to change the order of execution of the operators. Unless dictated otherwise by parentheses, complementation is done first, then intersection, and union is last, which is the conventional hierarchy for operators of this kind.

The surfaces available in MCNP include all of the surfaces of second degree in three dimensions plus certain tori. The general second degree surface is available. Its symbol is GQ and its equation is

$$E(X,Y,Z) = Ax^2 + By^2 + Cz^2 + Dxy + Eyz + Fzx + Gx + Hy + Jz + K = 0 . \quad (4)$$

A user specifies it by an input line like this:

surface no. GQ A B C D E F G H J K

Special simpler expressions with fewer coefficients are available for certain simple, frequently-used second degree surfaces. These include planes and cylinders, as shown in Fig. 1 and Table 1, and also spheres and cones.

The tori available are ones with elliptical cross section and with the axis parallel to one of the coordinate axes. They are rather handy in problems with inherently toroidal shapes, such as magnetically-confined-fusion machines.

TRACKING

When a particle comes out of the source or out of a collision, it is necessary to find the point where its track first intersects the boundary of the cell it is in. In Fig. 2, the collision is at K, and the track intersects the surfaces of the cell at A, B, C, and D. Intersection C is the required intersection with the cell boundary. MCNP calculates the intersections A, B, C and D by solving equations and accepting positive real roots. It then examines each intersection in increasing order of distance from the collision to find the cell boundary intersection. The algorithm used is shown by example in Fig. 2. A logical expression is set up parallel to the cell description but with the surface numbers replaced by true or false, depending on whether the collision point is on the designated side of the surface. At the collision point K, the value of the logical expression is, of course, true. As each intersection is examined, the logical values corresponding to the surface at the intersection are flipped and the expression is evaluated. As long as the intersections are still inside the cell, the value of the expression remains true. When it turns false, the cell boundary intersection has been found.

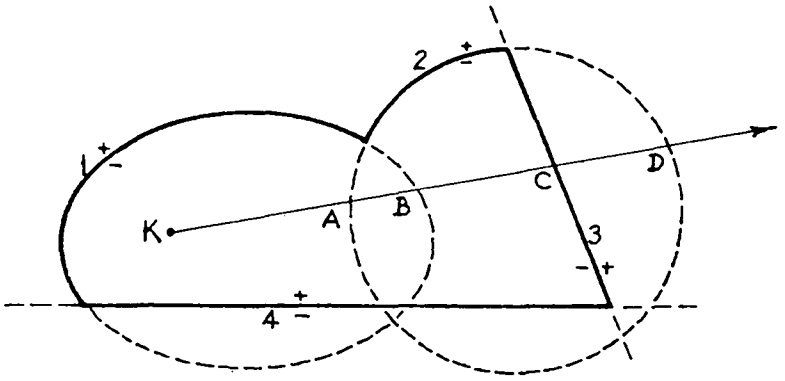

Logical expressions:

geometrical description of the cell:	(-1	: -2)	-3	4	
at collision point K:	(T	: F)	T	T	= T
across surface 2 at A:	(T	: T)	T	T	= T
across surface 1 at B:	(F	: T)	T	T	= T
across surface 3 at C:	(F	: T)	F	T	= F

Fig. 2. Tracking.

COMPARISON WITH OTHER GEOMETRY SCHEMES

The geometry scheme that MCNP once had was like the one described above except that it had no union or complement operators. I call it the surface list scheme since if the only operator is intersection, the specification of a cell is just a list of its bounding surfaces. The complement operator does not add a new capability, but it is a significant convenience. The union operator makes it possible to describe cells with concave edges and cells that consist of disconnected regions. Without the union operator, the two cells in Fig. 1 would have had to be eleven cells. A larger number of cells is not only more trouble to set up, which leads to setup errors, but in some cases complicates the tallying and the interpretation of the tallies.

In comparison with the other combinatorial geometry scheme with which I am familiar, the MCNP scheme differs mainly in the nature of the basic building blocks. In MCNP they are at once simpler and more general. I imagine that the scheme that turns out to be better for setting up a problem depends on the specific nature of the problem. The greater generality of the MCNP surfaces is a help in some cases. Also it must often happen that a body in combinatorial geometry is used for the sake of only one or two of its surfaces. The other surfaces then become parasites in tracking.

OTHER FEATURES

In some problems the geometry, or a significant part of it, is rotationally symmetric about some axis. In such cases the MCNP user may specify surfaces by giving the R and Z coordinates of a few points. Two points specify a cylinder or cone. Three points specify spheres, and ellipsoids, hyperboloids, and paraboloids of circular cross section.

MCNP may be used to rotate and translate surfaces from one coordinate system to another. Sometimes it is convenient to specify some of the surfaces in one coordinate system, such as by the point definition scheme described in the preceding paragraph. Then the code can be used to generate the coefficients that describe the surfaces in the main coordinate system of the problem.

Volumes of cells and areas of the portions of surfaces that bound cells are needed for normalizing tallies. MCNP has long been able to calculate these for cells rotationally symmetric about any axis. For other cells the user must enter the volumes and areas by hand. The code can, of course, be used in a separate run to calculate volumes by Monte Carlo in cases where it is hard to do it by hand. Recently the ability to calculate directly the volumes of polyhedral cells has been added to the code.

The code may also be used to plot pictures of the geometry on various computer graphics devices. The pictures are naturally very valuable to the users who are trying to check out their setups.

FUTURE IMPROVEMENTS

We intend to build a lattice capability into MCNP for better representation of geometries with repeated features.

We want to improve the plotting capability to show lines that are beyond the view plane, perhaps with perspective, instead of just pure cross sections of the geometry which is what we have now.

FLUX AT A POINT IN MCNP

E. D. Cashwell and R. G. Schrandt
Group X-6
Monte Carlo, Applications and Transport Data Group
Theoretical Applications Division
Los Alamos Scientific Laboratory
Los Alamos, New Mexico

ABSTRACT

The current state of the art of calculating flux at a point with MCNP is discussed. Various techniques are touched upon, but the main emphasis is on the fast improved version of the once-more-collided flux estimator, which has been modified to treat neutrons thermalized by the free gas model. The method is tested on several problems of interest and the results are presented.

INTRODUCTION

The next-event estimator (NEE) used in a normal Monte Carlo game for the flux at a detector embedded in a scattering medium suffers from a $(1/r^2)$-singularity. Consequently, the variance of the estimator is infinite even though the mean is finite.

In 1977, Kalli and Cashwell[1] proposed and evaluated three estimation schemes for flux at a point. A new, once-more-collided flux estimator (OMCFE) was proposed, which differed from those proposed by Kalos in his original paper.[2] The scheme has a $(1/r)$-singularity, leading to finite variance and $(1/\sqrt{N})$-convergence. It is based on a very simple p.d.f. of the path lengths in the sampling of the intermediate collision points. In addition, this simple p.d.f. for the path length was used in two schemes with bounded estimators similar to those proposed by Steinberg and Kalos[3] and by Steinberg.[4] The three schemes were evaluated in a realistic problem using the continuous energy Los Alamos Monte Carlo code MCNG, the forerunner of MCNP.[5]

Once-More Collided Flux Estimator (OMCFE)

In the present discussion we wish to focus on the OMCFE referred to above. This scheme has been incorporated into MCNP and, although some work still remains to be done, we wish to discuss this method in conjunction with other techniques available in MCNP.

The details of the OMCFE as it exists in MCNP are, for the most part, given in Ref. (1). Without repeating the treatment given there, we wish to touch on the main points of the method, as well as mention generalizations of the method to a wider class of problems. The OMCFE is superimposed on the particle history without affecting it. At each collision (or source point), a nonanalog game is played whereby a next collision point A is chosen, from which a contribution to the detector is made. That is, from every real collision point of the particle history, a once-more-collided contribution is made to the detector.

The two main features in determining the intermediate point A of the once-more-collided scheme are:

1. A directional reselection procedure based on the reselection technique of Steinberg and Kalos;[3] and

2. A nonanalog p.d.f. $p^*(s)$ which was used by Kalli[6] in 1972.

In Fig. 1, consider a collision at S with the resulting scattered direction $\vec{\Omega}_o$ in the cone described. Suppose that a new direction $\vec{\Omega}_1$ is chosen by sampling a new angle β_1 uniformly in $(0,\beta_m)$ and a ϕ_1 uniformly in $(0,2\pi)$. The result is a concentration of scattered directions closer to the line from S to the detector D than would normally occur. Of course, an adjustment factor must be applied to the weight of the particle due to the reselection.

Once the direction $\overline{\Omega}_1$ is chosen, suppose the intermediate point A is selected along this direction from the p.d.f. $p^*(s)$, where

$$p^*(s) = \frac{b}{(\pi/2 - \alpha_1)r^2} \quad \text{(Cf. Fig. 2).} \tag{1}$$

This density function corresponds to α being chosen uniformly in $(\alpha_1,\pi/2)$. Use of $p^*(s)$ leads to another weight adjustment $p(s)/p^*(s)$, where $p(s)$ is the analog p.d.f. for sampling distance to collision.

In the normal OMCFE, the point A is not a real collision point of the particle history. When these calculations involve reselection of direction and the distance to A using $p^*(S)$, as well as the normal next-event estimator, they tend to be time-consuming. In order to speed up calculations using the OMCFE:

1. Draw an imaginary sphere around the detector;

2. If the collision point S_i is outside the sphere but the direction after the collision is within the cone defined by S_i and the sphere, calculate the once-more-collided flux contribution by performing the directional reselection in the cone and calculate the intermediate point A by using $p^*(s)$;

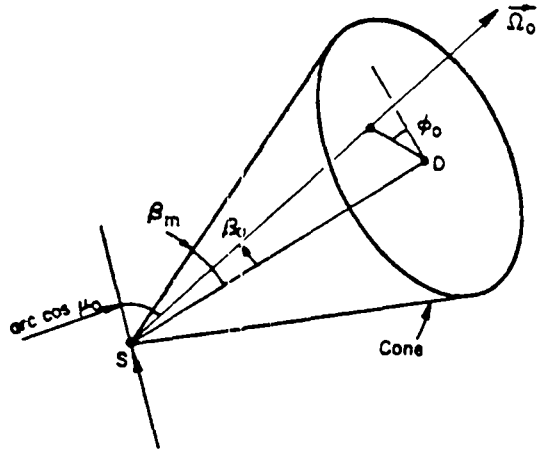

Fig. 1. Geometry in the reselection of a direction.

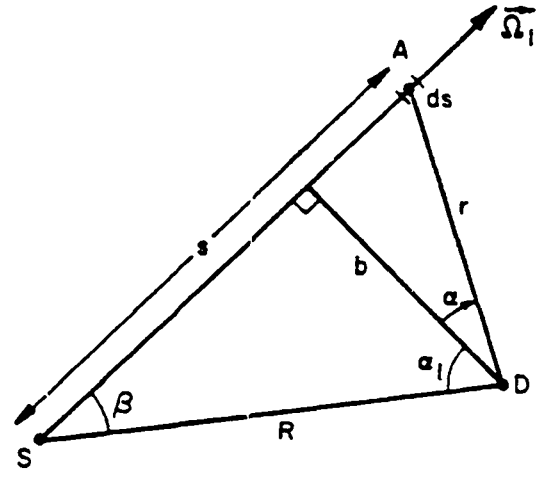

Fig. 2. Geometry in the selection of the intermediate collision point A.

3. If the collision point S_i is in the sphere and the direction $\vec{\Omega}_o$ after collision is in a 2π-cone (i.e., $\beta_o < \pi/2$) about the line from S_i to D, the once-more-collided contribution is calculated by reselection of $\vec{\Omega}_1$ and using p*(s) to determine the intermediate point A; if the direction $\vec{\Omega}_o$ after collision is such that $\beta_o > \pi/2$, no reselection is performed but the intermediate point A is chosen from p*(s); and

4. Otherwise, calculate the normal next-event contribution from the following collision point S_{i+1}.

The recipe as outlined above works very well in most problems containing ordinary materials. However, in non-thermal problems containing H, the forward scattering off H in the laboratory system of coordinates lead to some modification of the recipe because of the directional reselection procedure. Furthermore, the random motion of the target atoms combined with the motion of the neutron in the thermal routine using the free gas model in MCNP leads to rather extensive modifications for the same reason. The imaginary sphere around the detector may have to be reduced in size in the course of the calculation, as a result of using the reselection procedure.

With the necessary modifications, MCNP is able to treat problems of the types mentioned above, as illustrated by the sample calculations below. Several considerations led to the implementation of the OMCFE rather than one of the schemes leading to a bounded estimator in Ref. (1). First of all, the OMCFE was judged to be the simplest to insert into MCNP. Furthermore, the estimation of flux simultaneously at several points causes no problems in the OMCFE scheme. Finally, since the OMCFE does not alter the particle histories, its use has no effect on other tallies which may be required in a particular problem.

Let us describe briefly a subroutine, DXTRAN, which has been used in Los Alamos for some years and is an option available in MCNP.[5] We shall indicate its usefulness in our examples below. DXTRAN is of value in sampling regions of a problem which may be insufficiently visited by particle histories to yield adequate statistical accuracy in a given tally. To explain how the scheme works, let us consider the neighborhood of interest to be a spherical region surrounding a designated point P_o in space. In fact, we consider two spheres of arbitrary radii about the point $P_o(x_o,y_o,z_o)$. We assume that the particle having direction (u,v,w) collides at the point (x,y,z), as shown in Fig. 3. The quantities L, θ_I, θ_o, η_I, η_o, R_I, and R_o are clear from the figure. Let us somehow choose a point P_s on the outer sphere and assume that a scattered particle (let us call it a "pseudo-particle" for the moment) is placed there. We give this pseudo-particle a weight equal to the weight of the incoming particle at P_1 multiplied by the ratio of the p.d.f. for scattering from P_1 to P_s with no collision to the p.d.f. for choosing the point P_s in the first place.

If we sample directions isotropically in the cone defined by P_1 and the outer sphere, the number of directions falling inside the inner cone and the number falling in the outer cone will be proportional to $1-\eta_I$ and $\eta_I-\eta_o$, respectively. Let Q be a factor which measures the weight or importance which one assigns to scattering in the inner cone relative to scattering in the outer cone. We now proceed by the following steps:

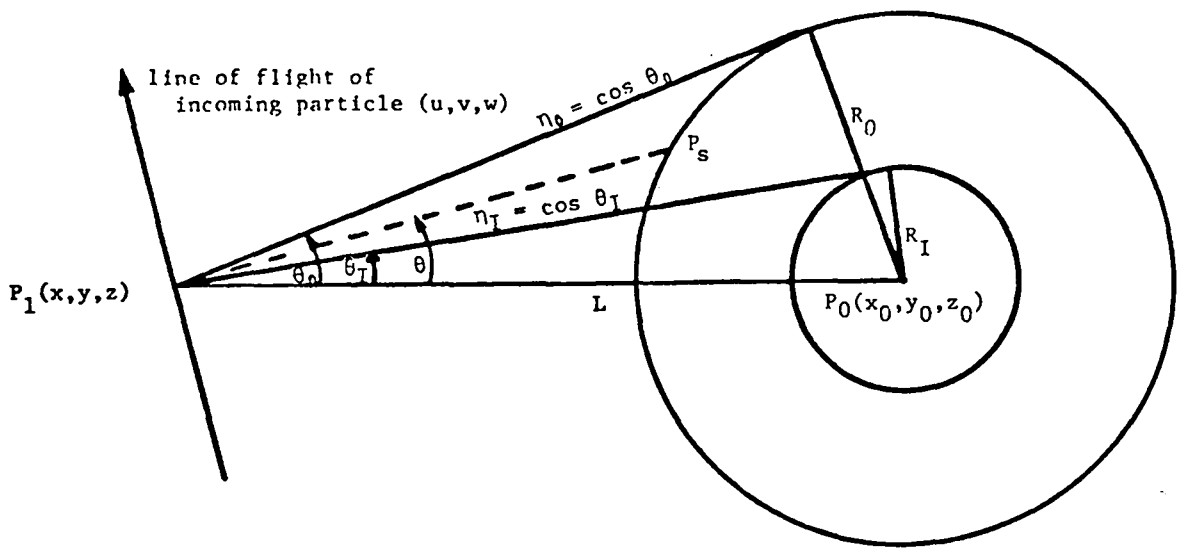

Fig. 3. The geometry of DXTRAN.

1. Sample η uniformly in $(\eta_I,1)$ with probability $Q(1-\eta_I)/[Q(1-\eta_I) + \eta_I-\eta_o]$; and with probability $(\eta_I-\eta_o)/[Q(1-\eta_I) + \eta_I-\eta_o]$ sample η uniformly in (η_o,η_I);

2. Having chosen θ from $\eta = \cos\theta$, we use the scattering formulas in the code to scatter through an angle θ (and an azimuthal angle ϕ chosen uniformly in $(0,2\pi)$) from the initial direction $\left(\frac{x_o-x}{L},\frac{y_o-y}{L},\frac{z_o-z}{L}\right)$, determining a new direction (u',v',w'). Advance the pseudo-particle in the direction (u',v',w') to the point P_s on the surface of the outer sphere. The new coordinates are saved;

3. The weight attached to the pseudo-particle is the weight of the particle at collision multiplied by

$$\nu \cdot \frac{P(\mu)\{Q(1-\eta_I) + \eta_I - \eta_0\} \exp\left\{-\int_{P_1}^{P_s} \Sigma_t(s)\, ds\right\}}{Q}, \quad \eta_I \leq \eta \leq 1$$

and

$$\nu \cdot P(\mu)\{Q(1-\eta_I) + \eta_I - \eta_0\} \exp\left\{-\int_{P_1}^{P_s} \Sigma_t(s)\, ds\right\}, \quad \eta_0 \leq \eta < \eta_I ,$$

where

$\mu = uu' + vv' + ww'$

$P(\mu)$ = p.d.f. for scattering through the angle $\cos^{-1}\mu$ in the lab system for the event sampled at (x,y,z).

ν = number of neutrons emitted from the event.

Since a collision supplies a particle (let us now drop the term pseudo-particle -- these particles are as real as any others) to the outer DXTRAN sphere, the particles from the collision at P_1 are picked up and followed further, but they are killed if they attempt to enter the sphere. It is apparent from the discussion above that this routine has certain features in common with a point detector routine.

This routine is used in a couple of the problems discussed below. In one problem, it is used to obtain the average flux in a small volume as a check against the result obtained from the OMCFE. In another, it is used to help get particles in the vicinity of a detector. While DXTRAN can be useful in many problems, it must be pointed out that the method is time-consuming, being similar in nature to a point detector routine. Further, attention must be paid to the problem of obtaining a sufficient number of histories in the vicinity of the DXTRAN sphere, not just inside the sphere.

CALCULATIONS

The problems discussed below were chosen to demonstrate the behavior of the OMCFE in a variety of settings, with some emphasis on the treatment of H and, in particular, its behavior in the presence of neutrons thermalized according to the free gas model. Illustrations of how DXTRAN can be useful, either as an aid to the OMCFE or as an aid in computing the average flux in a region with a track-length estimator, occur in two of the problems.

The geometries displayed in our problems are deliberately kept simple, partly so that we can display the so-called "exact flux", which is calculated very accurately (to a fraction of a percent) using a surface crossing estimator in the spherical geometry. In the schematics showing the geometry used, not every surface appears. Frequently, additional surfaces were added for the purposes of splitting and Russian roulette, or for the purpose of obtaining average flux in a region, but few surfaces were added in any one calculation.

In each problem, the source at the center of the sphere was chosen to be monoenergetic and isotropic in direction. As easily anticipated, it was found useful to use an exponential biasing to direct more particles toward the detectors. The latter were always placed on a radius of the sphere - say the positive x-axis. The initial flight of a neutron was chosen by sampling μ, the cosine of the angle the starting direction makes with the x-axis, from a p.d.f. $\sim e^{k\mu}$, with k a fixed parameter. The value of k used in each problem is listed on the schematic for that problem.

A feature of MCNP which was used in these calculations has to do with contributions to the detector D from collisions several free paths from the detector. E.g., when collisions occur more than x free paths from D, by playing Russian roulette one can permit, say, only one in ten collisions on the average to contribute to D, with weight enhanced by a factor of ten. The number x is set by the user and in these calculations was usually set to four. This feature of the code can save appreciable amounts of machine time in large systems.

Other information on the schematic which is of interest include the number density of atoms in the material used; the thermal temperature of the problem (if any); the average m.f.p. $\bar{\lambda}$, computed by MCNP over the course of the problem ; the source energy and energy cut-off (if any); the time on the CDC-7600 for a given sample of starting neutrons; and the imaginary sphere radii used in the OMCFE and in DXTRAN.

Figs. 4-12 display the geometries and graphs of the results for four problems. Table 1 gives a comparison of the final flux values at the end of each run with the "exact values". The errors in the final fluxes also appear.

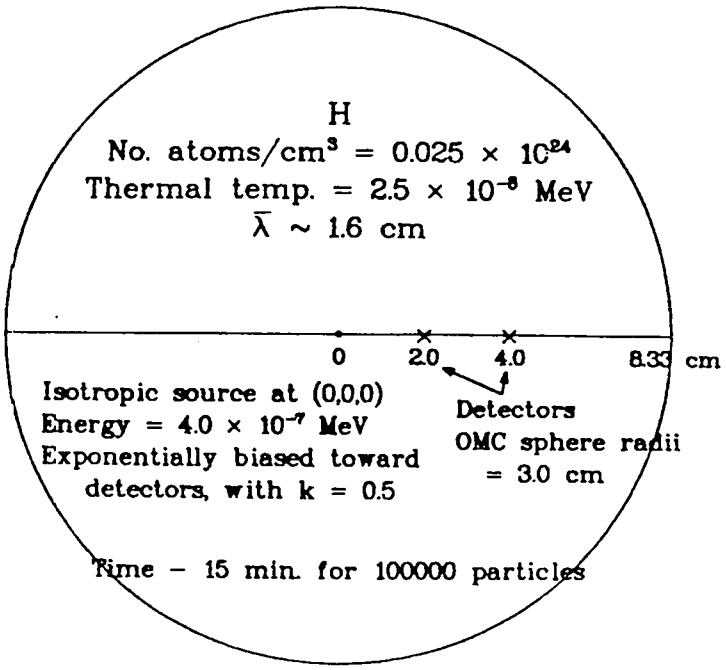

Fig. 4. Geometry for Thermal Hydrogen Problem.

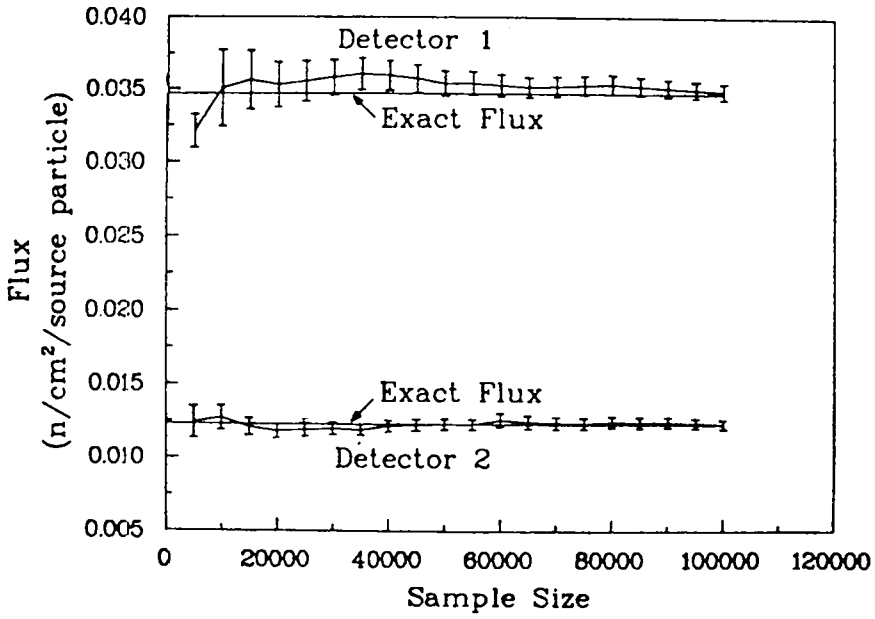

Fig. 5. Flux at Two Detectors in Thermal H with the OMCFE.

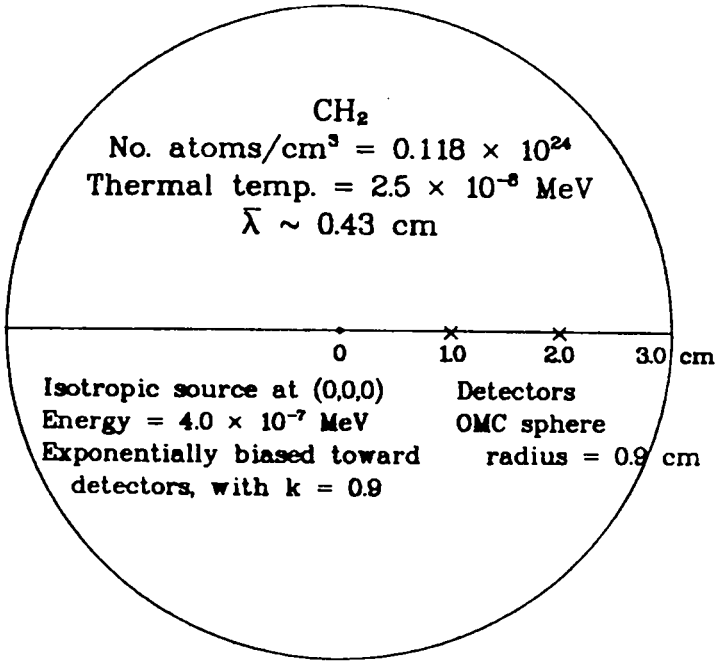

Fig. 6. Geometry for Thermal CH_2 Problem.

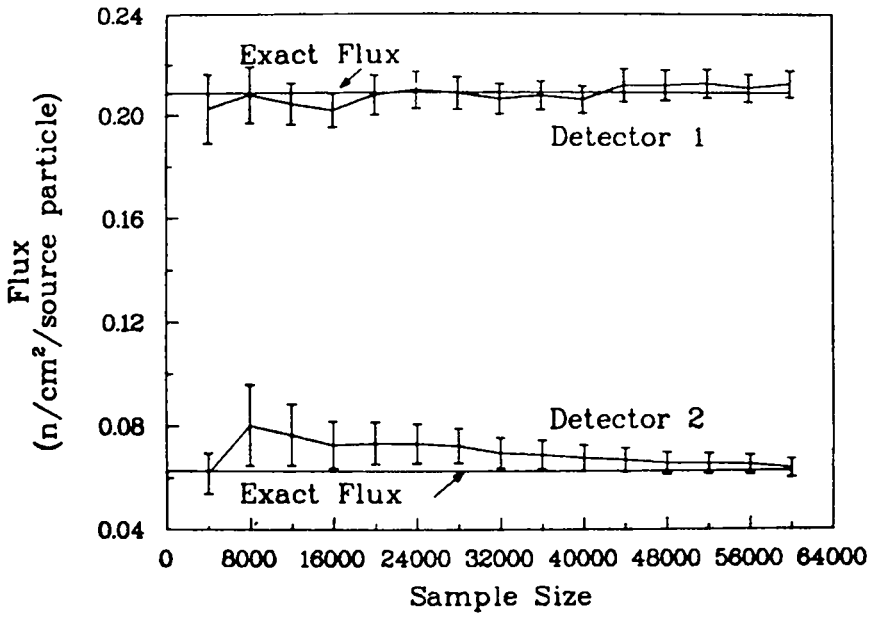

Fig. 7. Flux at Two Detectors in Thermal CH_2 with the OMCFE.

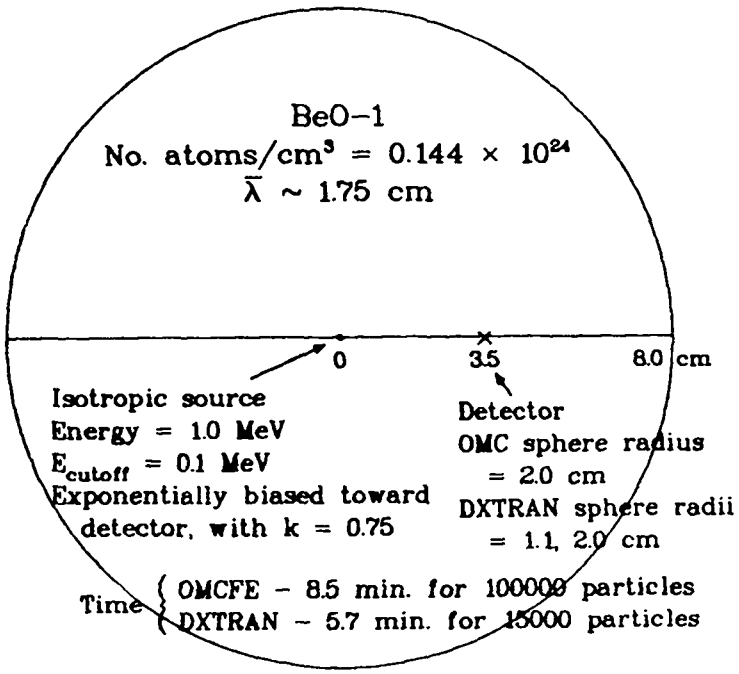

Fig. 8. Geometry for BeO-1 Problem.

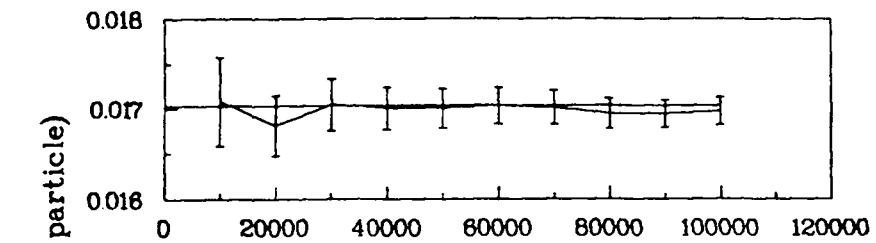

Fig. 9. Flux at a Detector in BeO-1 with the OMCFE.

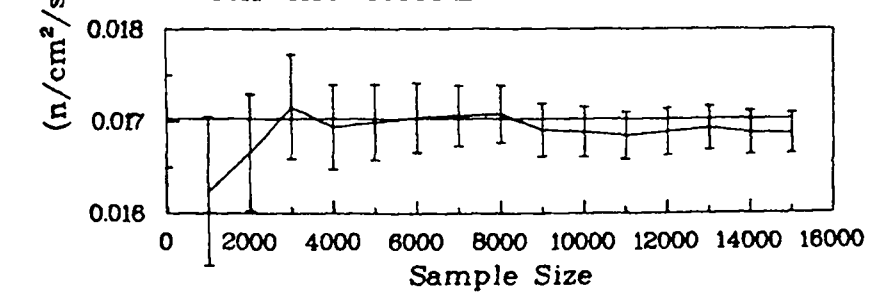

Fig. 10. Average Flux in the Vicinity of a Detector in BeO-1 Using DXTRAN.

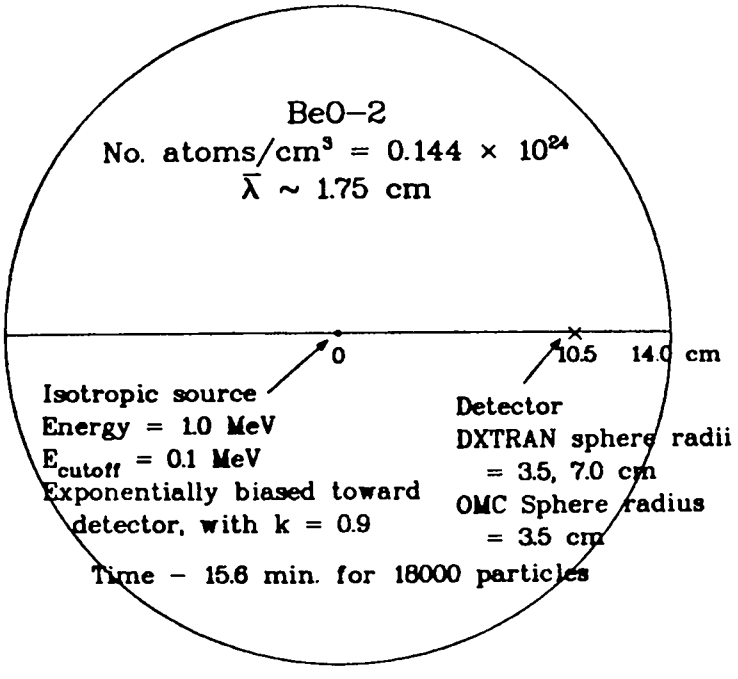

Fig. 11. Geometry for BeO–2 Problem.

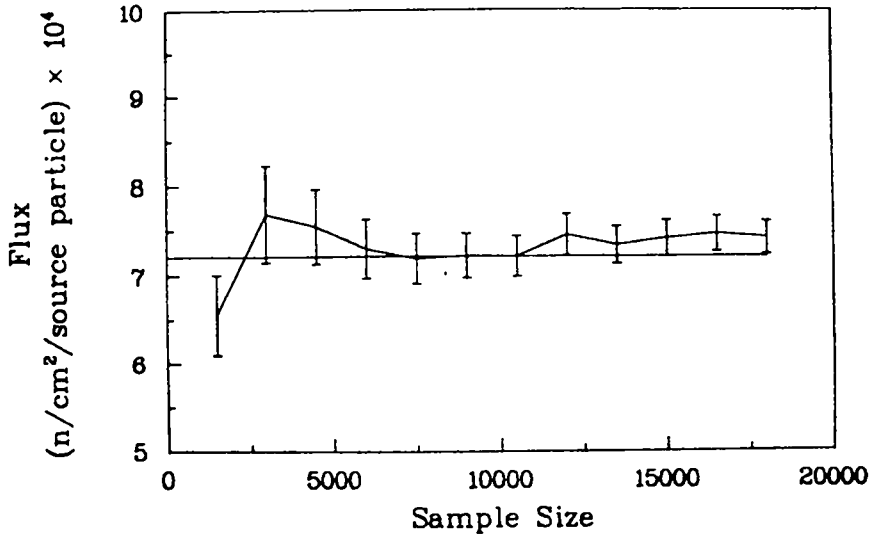

Fig. 12. Flux at a Detector in BeO–2 with the OMCFE and DXTRAN

TABLE I
Comparison of Calculated Flux with Exact Flux

		Flux (n/cm^2/source particle)			
		Exact (Surface Crossing Estimator)	OMCFE	Ave. Flux (Track Length Estimator)	Error (1 Standard Deviation)
Thermal H:	Detector 1	3.462×10^{-2}	3.486×10^{-2}		$.056 \times 10^{-2}$
	Detector 2	1.230×10^{-2}	1.231×10^{-2}		$.032 \times 10^{-2}$
Thermal CH_2:	Detector 1	2.086×10^{-1}	2.122×10^{-1}		$.053 \times 10^{-1}$
	Detector 2	6.259×10^{-2}	6.378×10^{-2}		$.357 \times 10^{-2}$
BeO - 1:	Detector 1	1.703×10^{-2}	1.697×10^{-2}		$.015 \times 10^{-2}$
	Detector 1	1.703×10^{-2}		1.687×10^{-2}	$.022 \times 10^{-2}$
BeO - 2:	Detector 1	7.207×10^{-4}	7.412×10^{-4}		$.185 \times 10^{-4}$

In Problem 1 the fluxes at two detector points in thermal H are calculated using the OMCFE. Problem 2 is a similar calculation in thermal CH_2. In Problem 3, the flux is calculated at a single detector in a sphere of BeO (non-thermal) for a source of 1 MeV neutrons at the center. The flux is first obtained using the OMCFE, and this is compared with an estimate of the average flux in a sphere about the detector of 1 cm radius. The latter estimate is obtained with the help of DXTRAN. Problem 4 finds the flux at a point in a BeO sphere situated approximately 6 free paths from the source using the OMCFE, but with the aid of a large DXTRAN sphere which encloses the detector. The error-bars (one standard deviation) on the points plotted indicate the statistical accuracy of the calculation in progress, as printed out by the code. The final results are, in every case, within a few percent of the value of the "exact flux" - in fact, the agreement appears somewhat better than expected in at least one case. For example, in the BeO-1 calculation the agreement between the exact flux and that obtained from the average flux in a sphere of 1-cm radius using DXTRAN is surprisingly good. Perhaps that is fortuitous - experience does not lead one to expect it in the average problem. The amount of computing time used could have been reduced in some cases without altering the results appreciably, but in dealing with estimates of flux at a point, it pays to be reasonably cautious. Quite frequently, the calculation is sensitive to the various parameters set in a problem - the size of the imaginary sphere in the OMCFE, the source bias, etc. Some care is essential in setting up a problem and a few short runs can be invaluable in making the necessary decisions, particularly in the case of a difficult problem.

Concluding Remarks

A very important method of estimating flux at a point in a problem with axial symmetry is through the use of a ring detector. MCNP contains a ring detector option and, although we did not use it in the present calculations, it should be mentioned as one of the tools available.

While the OMCFE in MCNP can deal with neutrons thermalized according to the free gas model, there remains the task of modifying the flux estimator to be compatible with neutrons thermalized with the $S(\alpha,\beta)$ treatment. It is hoped that this defect can be rectified in the not too distant future.

REFERENCES

1. H. J. Kalli and E. D. Cashwell, "Evaluation of Three Monte Carlo Estimation Schemes for Flux at a Point," Trans. Am. Nucl. Soc. 27, 370-371 (Nov. 27-Dec. 2, 1977). Also, Los Alamos Scientific Laboratory Report LA-6865-MS (September, 1977).

2. M. H. Kalos, "On the Estimation of Flux at a Point by Monte Carlo," Nucl. Sci. Eng. 16, 111-117 (1963).

3. H. A. Steinberg and M. H. Kalos, "Bounded Estimators for Flux at a Point in Monte Carlo," Nucl. Sci. Eng. 44, 406-412 (1971).

4. H. A. Steinberg, "Bounded Estimation of Flux-at-a-Point for One or More Detectors," Proc. NEACRP Meeting of a Monte Carlo Study Group, Argonne National Laboratory, July 1-3, 1974.

5. LASL Group X-6, "MCNP - A General Monte Carlo Code for Neutron and Photon Transport," Los Alamos Scientific Laboratory Report LA-7396-M, Revised Manual (November, 1979).

DEEP-PENETRATION CALCULATIONS

W. L. Thompson
O. L. Deutsch
T. E. Booth
Group X-6
Monte Carlo, Applications and Transport Data Group
Theoretical Applications Division
Los Alamos Scientific Laboratory
Los Alamos, New Mexico 87545

ABSTRACT

Several Monte Carlo techniques are compared in the transport of neutrons of different source energies through two different deep-penetration problems, each with two parts. The first problem involves transmission through a 200-cm concrete slab. The second problem is a 90° bent pipe jacketed by concrete. In one case the pipe is void, and in the other it is filled with liquid sodium.

Calculations are made with two different Los Alamos Monte Carlo codes: the continuous-energy code MCNP and the multigroup code MCMG. With MCNP, several techniques and combinations are evaluated: analog Monte Carlo, geometry splitting with Russian roulette, the exponential transformation, a weight window (constraining the upper and lower particle weights to be within certain limits), and using a combination of random walk/deterministic schemes. With MCMG, a comparison is made between continuous-energy and multigroup Monte Carlo and also between different multigroup scattering models (including the one used by the MORSE code).

Several unexpected results were found in the comparisons of the various calculations. For example, compared to continuous-energy calculations, multigroup calculations with standard cross-section weighting (for both Monte Carlo and S_n) underpredict the neutron leakage transmitted through the 200-cm concrete slab by a factor of four.

When considering different techniques for reducing the product of variance and computing time with regard to ease of use, reliability, and effectiveness, we find geometric splitting with Russian roulette to be a superior technique. The weight window, however, appears to be more effective than originally anticipated.

INTRODUCTION

Several Monte Carlo techniques are compared in the transport of neutrons of different source energies in two different deep-penetration problems. The first problem involves transmission through a 200-cm-thick concrete slab. The second problem is a 90° bent pipe jacketed by concrete. In one case the pipe is filled with liquid sodium, and in another case it is void.

In actual shielding applications, one might need to account for photon production and transport, streaming paths, the exact compositions of the shielding material including rebar, and other factors depending on the problem. For example, for 14-MeV neutrons incident on 200 cm of concrete, Oak Ridge concrete reduces the transmitted dose by a factor of ten better than does Los Alamos concrete. All the above considerations, however, are beyond the scope of this paper.

Rather than addressing particular and detailed shielding problems, the purpose of this paper is to apply different Monte Carlo techniques to problems of general interest to the shielding community and to compare the merits of the techniques. The problems considered here have nontrivial attenuations, and an attempt has been made to select representative features of real shielding problems without incorporating arbitrary or extraneous detail. In addition to a comparison of methods, results such as leakage, flux, and dose rate are presented, and we believe these results to be reliable. Doses throughout this paper refer to biological dose and were obtained with the ANSI[1] flux-to-dose conversion factors. By providing these benchmark-type results, others may wish to compare results from the same problems using different calculational tools. Interesting comparisons could be then made in terms of accuracy and efficiency between MCNP and other Monte Carlo codes (such as MORSE, TRIPOLI, or SAM-CE) and other calculational techniques such as S_n or hand calculations using buildup factors.

Basically, several techniques such as the exponential transformation and geometrical splitting with Russian roulette will be compared using the continuous-energy code MCNP[2] with virtually no approximations, MCNP with a pseudo-multigroup set of cross sections, and a true multigroup version of MCNP called MCMG.[3] All calculations done with MCMG are with 30 neutron energy groups. MCMG has the option to represent the distribution of scattering angles for group-to-group transfers by equiprobable cosine bins or by MORSE-type discrete scattering angles.[4] The pseudo-multigroup cross-section set in which the reaction cross sections have been collapsed into 240 energy groups for use with MCNP is referred to as the discrete-reaction data (DRXS). More details can be obtained about MCNP and MCMG in another paper by Thompson and Cashwell given at this seminar.

The amount of computer memory required for cross-section data for the ten constituents of ordinary Portland concrete is given in Table 1 as a function of calculational method, data set, and energy range.

About six hours of CDC-7600 computer time were used for the calculations reported in this paper. The multigroup calculations were done by Deutsch, Booth did the calculations with the exponential transformation and the weight window, and the rest of the calculations were done by Thompson.

Table 1. Neutron Cross-Section Storage for Portland Concrete

Mode	$Words_{10}$
MCNP, ENDF/B-V 20 MeV < E < 0.00912 MeV	297462
MCNP, ENDF/B-IV 20 MeV < E < 0.00912 MeV	133091
MCNP, DRXS (ENDF/B-IV) 20 MeV < E < 0.00912 MeV	42952
MCMG, 30 group 20 MeV < E < 10^{-4} eV	23000
MCNP, ENDF/B-V 20 MeV < E < 10^{-5} eV	310621
MCNP, ENDF/B-IV 20 MeV < E < 10^{-5} eV	139316
MCNP, DRXS (ENDF/B-IV) 20 MeV < E < 10^{-5} eV	45852
MCNP, ENDF/B-V 184 keV < E < 8.32 eV	56161

All calculations for this paper were done with ordinary Portland concrete as found in Schaeffer's book.[5] One calculation (the pencil-beam fission spectrum incident on a 100-cm-radius, 200-cm-thick concrete disk) was also done with the 04 concrete from the ANSI standard.[6] The compositions of these two concretes are listed in Table 2. The transmitted dose through the 04 concrete is 4.7 times higher than through the ordinary Portland concrete, while the transmitted leakage and flux are each about 5.2 times higher (these results are within 5%). All following reported results will be with ordinary Portland concrete.

Table 2. Concrete Compositions

Element	04 Wt.%	Portland Wt.%
H	0.56	1.00
O	49.81	52.9
Si	31.51	33.7
Ca	8.29	4.4
C	--	0.1
Na	1.71	1.6
Mg	0.26	0.2
Al	4.57	3.4
S	0.13	--
K	1.92	1.3
Fe	1.24	1.4
	ρ=2.339 g/cc	ρ=2.30 g/cc

All continuous-energy calculations were done with ENDF/B-V cross sections. However, the first problem that will be discussed, the pencil-beam fission spectrum incident on 100-cm-radius by 200-cm-thick concrete, wasalso done with ENDF/B-IV cross sections. There were no perceivable differences in any of the results. The Monte Carlo multigroup calculations were done with ENDF-IV cross sections. If calculations had been made involving heating or photon production, this conclusion of equality between IV and V may not have been true. Again, it is not the purpose of this paper to compare cross sections; this has been extensively done at Los Alamos[7,8] and elsewhere by others.

With regard to the use of different Monte Carlo techniques on a variety of applications, there are no universally valid prescriptions. The only truly effective rule of thumb is to always make two or three short, experimental runs (say of half a minute each) to help discover the characteristics of the particular problem and the effect of varying a parameter or two in a particular variance-reduction technique. There is no substitute for practical experience to guide the approach to a particular problem. What works in one situation in no way guarantees success in another situation and may even be harmful. A good Monte Carlo code should provide a variety of standard summary and diagnostic information to help understand what is happening in a given problem. In doing the calculations for this paper, we encountered some surprises to our intuition. However, short, preliminary runs provided the necessary insight for the final runs.

Finally, before getting down to business, comparisons between the various techniques will be done on the basis of a relative figure of merit, FOM = $1/(\sigma^2 t)$ where σ is the standard error associated with a result of the

calculation and t is the computer time required. For example, if it took 30 minutes to get a 4% error, 20.8 is the figure of merit. Note that to compare your FOM to the ones reported in this paper, you will also need to factor in the speed of your computer system relative to ours. All calculations reported by us were done on a CDC-7600 computer. All reported errors represent one standard deviation. Note that there is also an error associated with the figure of merit, a variance of the variance. In the following calculations, we attach no significance to small differences in the FOM such as between 62 and 55.

The factor $\sigma^2 t$ is directly related to the dollar cost of running a job. It is important to note that the cost depends both on σ^2 and t; for example, you may reduce σ^2 but only at a greater expense in t or vice versa; the product of the two must be reduced to be beneficial. Not explicit in this relation for the total cost of a job is the cost in human time to set a job up and the cost of the preliminary experimental runs to set the parameters. If you spend three days with an elaborate setup and five hours of computer time refining and optimizing the parameters in the best possible way so that your job runs in 10 minutes rather than 20, you have lost. In all the following calculations, we usually made two or three preliminary runs for about a half minute each. We make no claim that our setups and figures of merit are the best, but they are acceptable as being cost-effective. Undoubtedly, someone can make improvements but probably not without diminishing returns.

VARIANCE-REDUCTION TECHNIQUES

The successful application of the Monte Carlo method to any deep-penetration problem generally requires the use of one or more variance-reduction techniques. In general, one can expect that some techniques or combinations of techniques will be more effective than others in terms of range of applicability, ease of use, reliability, and performance. We measure performance in terms of the figure of merit $1/(\sigma^2 t)$. By reliability, we refer to the possibility of injudicious selection of the parameters of a technique resulting in erroneous answers because an important part of phase space may not have been sampled adequately, if at all. Finally, ease of use refers to the degree of difficulty in determining the parameters of a technique and to the sensitivity of performance to precise selection of the optimal parameters.

Based on many years of experience and observations of users at Los Alamos, the most frequently-used techniques at Los Alamos are geometry splitting with Russian roulette, directional source biasing, survival biasing, and a weight-cutoff game incorporating Russian roulette. These techniques are frequently used in combination. It is assumed that if nenrgy and/or time cutoffs are appropriate for a problem, then they have been used also. The exponential transformation is infrequently used, and in fact, we have discouraged its use. We note all too frequently that the less experience a user has, the more any of the variance reduction

techniques are abused by using the techniques inappropriately, or with several techniques in conjunction leading to conflicts, or most commonly by biasing too heavily. Any of these problems can result in a wrong answer. It cannot be overemphasized that any variance-reduction technique must be used with caution and understanding.

In the following calculations, several different techniques are tried and compared. For all problems, we compare geometry splitting with Russian roulette, the exponential transformation, a weight window, and DXTRAN. The effect of running the problems in a purely analog fashion will also be illustrated. Other techniques will also be tried but not for all cases. A short description will be given for the main techniques used in these calculations.

A more detailed description can be found in Ref. 2.

Geometry Splitting with Russian Roulette

MCNP does not split particle tracks upon collision but as a function of spatial location. The geometry is subdivided into several cells, and each cell is assigned an importance. When a track of weight W passes from a cell of importance I to a cell of higher importance I', the track is split into I'/I tracks, each of weight WI/I'. (Non-integer splitting is allowed, but we will consider only integral importance ratios for simplicity.) If a track passes from a cell of importance I' to a cell of lower importance I, Russian roulette is played; a track survives with frequency I/I' and is assigned a new weight of WI'/I if it survives. Generally, the source cell has importance of unity, and the importances increase in the direction of the tally. The importances are chosen to keep the track population roughly constant between the source and the tally.

Weight Cutoff with Russian Roulette

The weight cutoff is made relative to the ratio of the importance of the source cell to the importance of the cell where weight-cutoff is about to take place. This keeps the geometry-splitting and weight-cutoff games from interfering. If a track's weight falls below quantity WC2 (usually from survival biasing), Russian roulette is played. A track survives with frequency WC2/WC1 and is assigned the weight WC1 if it survives. WC1 and WC2 are generally chosen to be 0.5 and 0.25, respectively, for a starting weight of unity but are problem-dependent.

Exponential Transformation

This technique allows a track to move in a preferred direction by artificially reducing the macroscopic total cross section in the preferred direction and increasing the cross section in the opposite direction according to

$$\Sigma_{ex} = \Sigma_t(1 - p\mu) \quad , \tag{1}$$

where

Σ_{ex} = transformed total cross section,
Σ_t = true total cross section,
p = parameter used to vary degree, of biasing, $0 \leqslant p < 1$, and
μ = cosine of angle between preferred direction and track's velocity.

Upon collision, the track weight is multiplied by

$$w_c = \frac{e^{-p\Sigma_t \mu s}}{1 - p\mu} \quad , \tag{2}$$

where s is the distance to collision. Note this can lead to a dispersion of weight, and that it is possible for some weights to become very large if the tracks are traveling opposite to the preferred direction.

We have found the exponential transformation by itself to be of limited use. The dispersion of weights that it creates can result in an unreliable sample mean while the sample variance may erroneously indicate an acceptable precision. Furthermore, it is not clear how to choose the biasing parameter p, but we note that it is generally chosen too high - especially by novice users. For the calculations of this paper, the parameter was selected by observing the sample variance as a function of the parameter on a few short runs.

When combined with a weight window to place a bound on the upper and lower weights of tracks, we have found that the exponential transformation can be useful. However, choosing parameters for the weight window can further complicate the problem setup, especially for the inexperienced user.

Weight Window

A weight window consists of an upper and a lower bound for a particle's weight. If the track weight is less than the lower weight bound, Russian roulette is played and the weight is increased to lie inside the window or the track is killed. If the track weight is above the upper bound then the track is split so that the resulting tracks have their weights within the window. The bounds of the window can be set as a function of energy and spatial position.

This weight-window capability is presently not a permanent feature of MCNP. It is available as a modification and is under evaluation by Group X-6. Among other things, we are trying to learn how to use it. It appears that this technique has merit not only when used with the exponential transformation but in conjunction with other techniques. The bane of any variance-reduction technique is creating a dispersion of weights and especially creating a few tracks with very large weights. The weight window appears to reduce these problems effectively.

DXTRAN

In a geometry region which is difficult to sample adequately, the DXTRAN scheme of MCNP can be of value. At each collision, contributions of scattered particles are deterministically transported to a spherical neighborhood of interest. These contributions, or pseudo-particles, are placed on a sphere surrounding the neighborhood of interest and then transported in the ordinary random-walk manner. The parent particle giving rise to the pseudo-particle at a collision continues its random walk, but it is killed if it tries to enter the neighborhood during its random walk.

There are actually two DXTRAN spheres. The pseudo-particles are placed on an outer sphere. An inner sphere concentric to the outer one is used to bias the placement of pseudo-particles within the cone defined by the inner sphere and the point of collision.

DXTRAN has certain features in common with a point detector. It also has the disadvantages of a detector: it can significantly increase computation time, and it is susceptible to large-weighted contributions. For these and other reasons, success is not guaranteed when using DXTRAN, and it (like a detector) should be used selectively and carefully.

A useful feature of MCNP is the DD input card. This provides diagnostics pertaining to DXTRAN or point detectors such as the accumulative fraction of the number of contributions, the fractional contribution, and the accumulative fraction of the total contribution - all as a function of mean free path away from the DXTRAN sphere or detector. Having this information from a short run, Russian roulette can be played on contributions a selected number of mean free paths away. This can save substantial computer time.

Angle Biasing

Angle biasing for the problems of this paper was not applied for two reasons: (1) our experience with angle-biasing techniques is both limited and discouraging, and (2) angle biasing is not a standard MCNP option. We have experience with sampling two different (fictitious) exit densities, namely

$$p_1(\Omega) = \frac{1 + bv}{4\pi} \quad = \text{probability of sampling a unit solid angle about } u,v,w \quad |b| \leq 1 \tag{3}$$

and

$$p_2(\Omega) = \frac{be^{bv}}{e^{b} - e^{-b}} \frac{1}{2\pi} = \text{probability of sampling a unit solid angle about } u,v,w \quad b > 0. \tag{4}$$

Both of these schemes seem to introduce a large variation in particle weights which is reflected in a poor variance of the sample mean. Use of weight window improves the variance, but only to the point where the variance matches that of the weight window alone.

It is entirely possible that other angle-biasing schemes may perform much better. In particular, angle-biasing schemes in discrete-angle Monte Carlo codes (such as TRIPOLI) can be easily fabricated to avoid large variations in particle weights. This does not appear to be the case in continuous-angle Monte Carlo codes (such as MCNP).

CONCRETE-SLAB PROBLEMS

A major advantage of Monte Carlo is the ability to calculate with no compromise in geometrical reality. Since the purpose of this paper is to illustrate some variance-reduction techniques, this advantage plays no role in this particular problem. S_n is more appropriate for this problem - but at the possible expense of getting the wrong answer because of the multigroup approximation (as will be seen later in this paper).

This problem consists of two parts. Both parts consist of a 200-cm-long homogeneous cylinder of ordinary Portland concrete with a pencil-beam source of fission-spectrum neutrons incident along the axis. In one case the radius of the cylinder is 100 cm, and in the other the radius of the cylinder is 20 cm. The object is to tally the net neutron leakage (or current) across the face opposite the source for comparison of all the methods. However, the transmitted flux and biological dose were also calculated by MCNP. The geometry of both cases is illustrated in Fig. 1.

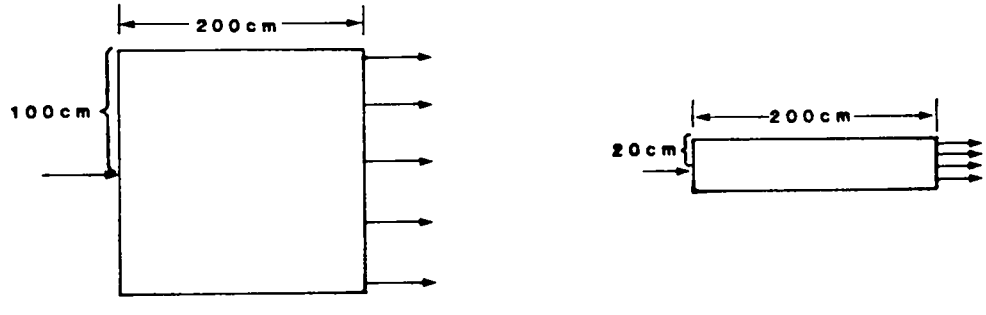

Figure 1. Concrete Slab Problems.

The source energy spectrum is defined according to the Maxwellian representation of the fission spectrum:

$$f(E) = \frac{2}{\sqrt{\pi}T}\sqrt{\frac{E}{T}}\, e^{-E/T} \quad , \tag{5}$$

where we have chosen the parameter T = 1.30 MeV that produces an average source energy of 1.95 MeV. A prescription that was used to sample from

this spectrum for MCNP is in the Appendix. For the multigroup calculations with MCMG, the spectrum was analytically integrated to determine the group sources:

$$\int_{E_{g+1}}^{E_g} f(E)\, dE = \frac{2}{\sqrt{\pi}} \left[\sqrt{\frac{E_{g+1}}{T}}\, e^{-E_{g+1}/T} - \sqrt{\frac{E_g}{T}}\, e^{-E_g/T} \right] + \left[\mathrm{erf}\left(\sqrt{\frac{E_g}{T}}\right) - \mathrm{erf}\left(\sqrt{\frac{E_{g+1}}{T}}\right) \right] . \tag{6}$$

The group sources are listed in the Appendix.

A short adjoint run with MCMG plus an S_n calculation indicated that source particles below 3.68 MeV (this corresponds to one of the multigroup boundaries) made few tally contributions. More precisely, about 10% of the transmitted leakage results from source neutrons below 3.68 MeV. Therefore, the source spectrum was sampled for energies only above 3.68 MeV. These high-energy-source particles account for 12.929% of the total source particles in the unaltered spectrum. Therefore, all results were multiplied by 0.12929 to normalize to one total source neutron. By biasing the source in this manner, the figure of merit for MCNP calculations increased by a factor of two.

For the 3.68-MeV truncated fission spectrum, 200 cm of concrete is about 25 mean free paths thick; for the full, unaltered spectrum, the 200-cm-slab is about 28 mean free paths. In the first 10 cm, the average mean free path is about 6 cm. After only a few more centimeters into the concrete though, the average mean free path becomes about 4.5 cm and remains very close to this throughout the 200-cm thickness. The energy cutoff for the calculations was set at 0.00912 MeV (again this corresponds to one of the group boundaries) because only a couple of percent of the transmitted neutron dose comes from transmitted neutrons with an energy less than this. Using this cutoff increases the figure of merit by a factor of about three. There are 18 groups in the multigroup data above 0.00912 MeV. Furthermore, this energy cutoff requires a smaller computer-memory requirement.

To illustrate the effect of the above energy cutoffs and photon production and that the simplification for this academic paper may not be valid for actual shielding problems, MCNP was used for a 10-minute calculation with none of the above cutoffs and also accounted for photon production for a 100-cm radius by only a 100-cm-thick concrete slab. The figure of merit for the total neutron dose is 8.6 using splitting, and the total neutron dose is $8.1 \times 10^{-13} \pm 8.5\%$ mrem/source neutron. The dose from transmitted neutrons above 0.01 MeV is 7.5×10^{-13}, and the total photon dose is $1.7 \times 10^{-13} \pm 8.5\%$ mrem per source neutron. About 49% of the photons were started in the energy range 2-5 MeV, 2.7 MeV of photon energy were started on the average per neutron, and the average weight of photons started was 0.87 per neutron. Another run was made but with the neutron energy cutoff at 0.01 MeV. The figure of merit increased to about 56, the total neutron dose became $7.2 \times 10^{-13} \pm 6\%$, and the photon dose dropped to $2.6 \times 10^{-15} \pm 18\%$. Now about 14% of the photons start between 2 and 5 MeV,

0.24 MeV of photon energy were started per neutron, and the average weight of photons started was 0.14 per neutron. For 14-MeV neutrons incident on 100 cm of concrete and using no cutoffs or approximations, about 8% of the total dose comes from photons.

100-cm-Radius Problem

With the pencil-beam source, the axially penetrating leakage is $8.2 \times 10^{-9} \pm 4.4\%$, the transverse leakage is 1.9×10^{-5}, and the backscatter leakage is about 35%. Because of the negligible transverse leakage, the problem geometry is equivalent to a homogeneous, semi-infinite slab. About 9.5% of the neutron weight is lost to capture.

In a purely analog case (no splitting, survival biasing, or anything else), except for source energies greater than 3.68 MeV, 21484 source neutrons were started in two minutes of computer time. At 50 cm there were 5409 (25%) neutrons, 83 were at 100 cm, and none were at 150 cm. This is a very clear example of why variance-reduction techniques are necessary.

Adding survival biasing and weight cutoff with WC1 = 0.5 and WC2 = 0.25 to the above example, a slight improvement is noticed in the same two minutes of time: 19336 source particles were reduced to 5477 (28%) at 50 cm, to 102 at 100 cm, and to none at 150 cm. Only three tracks were lost to the Russian roulette part of the weight cutoff game. With WC1 and WC2 increased to 1.0 and 0.5 respectively, 19432 source particles were reduced to 5461 (28%) at 50 cm, to 106 at 100 cm, and to none at 180 cm. Only 121 tracks were lost to Russian roulette. In this problem survival biasing and weight cutoff help a little but not a significant amount. It is a generally accepted practice, however, to use these two techniques routinely (naturally there are exceptions).

To add geometry splitting with Russian roulette, the concrete cylinder was subdivided axially into cells 10-cm-thick by adding plane splitting surfaces; 10 cm was chosen because it is a convenient number and because it allows a couple of mean free paths between splitting surfaces (based on an average of 4.5 cm for a mean free path averaged over collisions). Cell thicknesses of 15 cm worked equally well. The problem was run for half a minute with the importances of all cells set to unity. Part of the standard summary output of MCNP is the track population in each cell, and wherever the population dropped by a factor of two, the importance of that cell was doubled relative to the adjacent cell in the direction of the source. In some places the two-for-one splitting was not enough, so four-for-one splitting was occasionally used. If an incremental cell thickness less than 10 cm had been chosen, two-for-one splitting could have been used throughout. Conversely, greater than 10-cm increments would have led to a more consistent use of four-for-one splitting. A goal is to try to keep the population roughly constant, say within 50%.

For this particular problem, there appears to be little difference in computer efficiency between two-for-one and four-for-one splitting. Other ratios can also be used as necessary. Two-for-one splitting makes it

easier to level the population, but it requires the user to add more cells and surfaces to the problem setup. Four-for-one splitting requires less input from the user and less arithmetic for the computer, but it is harder to level out the population. Going beyond four-for-one splitting introduces greater risk because that implies a fairly large reduction in the population before it is built back up. The danger is that once a sample population deteriorates to a small size, source information associated with the sample can be lost. Once information is lost, it can never be regained. For example, in the analog problem mentioned earlier, at 170 cm we could have introduced the first splitting surface and split 21484-for-one. The track population would be back to its original size, but then the true energy spectrum would be represented by one discrete energy. The old saying about squeezing blood out of a turnip is very appropriate here.

Three iterations of half a minute each were used to set the importances. The ratio of importances between cells, the actual importance assigned to a cell, and the track population in each cell are shown in Table 3 for 91440 source neutrons. In this final run, weight cutoff was played with WC1 = 0.5 and WC2 = 0.25 (both times the starting weight of the neutrons), resulting in 4233 tracks lost to Russian roulette. In the splitting game, 1118990 tracks were created, but 460729 were lost to Russian roulette. Note that in cell 18 the population is too high.

Table 3. Splitting in the 100-cm-Radius by 200-cm-Thick Concrete Problem

Cell	Importance Ratio	Importance	Track Population
(Source) 1	1	1	94215
2	1	1	69498
3	2	2	86168
4	2	4	86972
5	2	8	82441
6	2	16	78332
7	4	64	140593
8	2	128	118175
9	2	256	101254
10	2	512	86628
11	2	1024	75750
12	4	4096	127292
13	2	8192	102290
14	2	16384	89315
15	4	65536	151848
16	2	131072	123118
17	2	262144	107322
18	4	1048576	180848
19	2	2097152	142741
(Tally) 20	2	4194304	109876

For this problem the transmitted leakage is $8.21 \times 10^{-9} \pm 4.4\%$ for neutron leakage, the transmitted dose is $1.22 \times 10^{-17} \pm 4.5\%$ mrem per source neutron, the transmitted flux is $4.10 \times 10^{-13} \pm 4.3\%$ neutrons/cm^2, the leakage escaping through the curved cylindrical surface is $1.91 \times 10^{-5} \pm 16\%$ neutrons, the backscattered leakage is $4.51 \times 10^{-2} \pm 0.4\%$, and 6.7 is the figure of merit.

Other splitting games can also be played. The most obvious is a combination of axial and radial splitting. With radial splitting, one could set up a cone as a splitting surface with its vertex at the source point and then intersecting the edge of the exit face. Secondly, rather than a cone, a concentric cylinder could be used with its radius half that of the outer cylinder. It turns out that neither of these approaches results in much (if any) gain in this problem. What small amount is gained in reducing σ^2 is lost by an increase in t because of the added arithmetic for the computer.

There is a frequently-heard rule of thumb for geometry splitting that says split two-for-one every mean free path, but you do not hear if this means a mean free path based on source energy or average energy of the particles in the geometry. In this problem, a mean free path based on a source energy is about 8 cm and about 4.5 cm averaged over collisions. Splitting two-for-one every 4.5 cm in only a 100-cm-thick slab of concrete, 1 source neutron had been split into a population of 440 at 50 cm and 12740 at 100 cm and required 0.96 minutes of computer time. Splitting two-for-one every 8 cm in a similar 100-cm-thick slab of concrete was better; 335 source neutrons required 0.52 minutes of computer time and were split into a population of 1597 at 50 cm and 1904 at 75 cm. Obviously, this rule of thumb applied by either method leads to oversplitting.

Using the weight window with only survival biasing and nothing else, the transmitted leakage is $8.26 \times 10^{-9} \pm 9.3\%$ with 6.3 for a figure of merit. The lower weight bound in the source cell was chosen to be 50% lower than the particles' source weight. The lower weight bound for the rest of the cells was chosen to be a factor α less than the previous cell's lower weight bound where α for cell i was chosen as

$$(\text{starting weight})\alpha^i = \text{transmission obtained by previous short run.} \tag{7}$$

The upper weight bound was chosen to be five times the lower weight bound.

Using the exponential transform with survival biasing, no weight-cutoff game, and a transform-biasing parameter of 0.7, only a very short run was required to see a poor performance. The figure of merit was 1.5, and the transmitted leakage was $4.86 \times 10^{-8} \pm 39\%$ which is too high by a factor of six - in other words, completely unreliable.

Adding to the exponential transformation a weight-cutoff game (but not the weight window) that is dependent on cell importances had the result that after 4.6 minutes of computer time the transmitted leakage was

$5.22 \times 10^{-9} \pm 19.2\%$ with a figure of merit of 4.2; after 10 minutes, $8.22 \times 10^{-9} \pm 26.7\%$; and after 17.6 minutes the leakage was $8.06 \times 10^{-9} \pm 18.4$ with 1.7 as the figure of merit. This example demonstrates the value in watching the behavior of a sample mean and its variance during the progress of a calculation. If either is unstable, the sample mean is unreliable. By not watching this behavior, a result (such as the leakage of 5.22×10^{-9}) may be incorrectly accepted as satisfactory based on an apparently low variance.

Applying the weight window and exponential transformation together produced the best of all results with a figure of merit of 22.6 and a transmitted leakage of $8.49 \times 10^{-9} \pm 3.0\%$.

The multigroup code MCMG using 30 groups and geometry splitting determined in the same manner as for MCNP was used on this problem. The figure of merit was 11.9, but the transmitted leakage was $2.17 \times 10^{-9} \pm 5.6\%$ which is low by a factor of four. Both the continuous-scattering angle and MORSE discrete-scattering angle treatments were used. No difference between the two was observed. For optically thin transmissions, however, the continuous treatment is superior.

MCNP itself can be used in a pseudo-multigroup fashion by using our discrete reaction cross-section set DRXS. These cross sections are equivalent to the regular continuous-energy cross sections used by MCNP except that the reaction cross sections have been collapsed into 240 energy groups. Using MCNP and these discrete cross sections along with geometry splitting on this problem, the transmitted leakage is $5.08 \times 10^{-9} \pm 6.8\%$ with 8.0 for the figure of merit.

All of these results are summarized in Table 4.

To our surprise, the performance of the weight window may be relatively insensitive to the size of the window. This problem was tried with the ratio of the upper to lower bound set at 400 to compare with the ratio of 5 used throughout this paper. The factor of 400 is consistent with a similar scheme used in MORSE. The results were virtually unchanged; the figure of merit was 19.5 and the leakage was $7.89 \times 10^{-9} \pm 10.6\%$. This implies that it is a very few tracks with very large weights that cause tallying problems. The problems caused by a weight dispersion have long been recognized, but the true nature of the dispersion may not have been fully appreciated.

The dramatic improvement in the performance of the exponential transform when it is used in conjunction with splitting at an upper weight limit seems to indicate that a substantial fraction of the tally variance is associated with very high-weight particles. Particles can accumulate a high weight by traveling against the transform vector for part of their trajectory. With splitting at the upper weight limit, the distribution of tally scores per source particle for each high-weight particle is shifted from a binary distribution of scoring or not scoring in one lump to a superposition of binary distributions with smaller components. The net

result is to reduce the variance while leaving the tally mean unchanged. The computational time involved is relatively small because the high-weight particles are relatively infrequent, and so a net gain is achieved in the figure of merit.

The biggest surprise we had in doing the calculations for this paper was the disagreement between the continuous-energy and multigroup results. We see from Table 4 that the MCMG multigroup results underpredict the continuous-energy results by a factor of almost 4. The group cross sections consist of 30 neutron groups from the ENDF/B-IV evaluation with a weighting spectrum which is a fission spectrum matching a 1/E spectrum for the energy range of interest.[9] In Table 5 we compare the partial leakage J^+ in the direction of penetration at 15-cm intervals through the concrete for continuous-energy and multigroup-collision treatments. It can be seen that the discrepancy appears to grow systematically. The column labeled "DRXS" is a calculation with the 240-group discrete-reaction cross sections using MCNP. The results of the DRXS calculations fall in between the continuous-energy and the 30-group MCMG results. One may conclude that an energy self-shielding effect introduces a discrepancy into the multigroup results and that the magnitude of the discrepancy may be quite significant for deep-penetration applications using standard cross-section sets. Although this effect has been reported in transport through pure materials (most notably in thick iron shields), it might not be expected in mixtures such as concrete with significant masking of cross-section windows and the presence of hydrogen to lessen the importance of windows.

Table 4. Summary of Results for 100-cm-Radius by 200-cm-Thick Concrete Cylinder

Method	Transmitted Leakage	% Error	FOM	Computer Minutes
MCNP, splitting	8.21×10^{-9}	4.4	6.7	77
MCNP, weight window	8.26×10^{-9}	9.3	6.3	18.4
MCNP, exponential transformation	4.86×10^{-8}	39	1.5	4.4
MCNP, exponential transformation and weight cutoff	8.06×10^{-9}	18	1.7	17.6
MCNP, exponential transformation and weight window	8.49×10^{-9}	3.0	22.6	49.2
MCMG, splitting	2.17×10^{-9}	5.6	11.9	26.8
MCNP, discrete reactions, splitting	5.08×10^{-9}	6.8	8.0	27.0

Given the discrepancy between continuous-energy and multigroup Monte Carlo, an obvious question becomes what is the result of an S_n calculation. Therefore, we made an S_n calculation with the one-dimensional S_n code ONETRAN.[10] The geometry was assumed to be a 200-cm Portland concrete slab of infinite lateral extent. An infinite extent is a very good approximation since the Monte Carlo calculations indicated the transverse leakage to be about 2×10^{-5}. Using the truncated fission spectrum (i.e., source energies greater than 3.68 MeV) and the same 30 group ENDF/B-IV cross-section set as used with MCMG, good convergence was achieved with ONETRAN using Δr of 1.66 cm and an S-8 Lobatto quadrature; the leakage was 2.45×10^{-9}. Using the full fission spectrum source, the leakage was 2.71×10^{-9}. Good convergence with a Gauss quadrature was not achieved until an S-16 or greater quadrature was used. There are a couple of conclusions: (1) S_n agrees with the MCMG result of $2.17 \times 10^{-9} \pm 5.6\%$ within two standard deviations, and (2) S_n requires a Lobatto or high-order Gauss quadrature for good convergence in deep-penetration problems.

To verify that the transverse leakage was truly negligible and that the one-dimensional S_n and MCMG results were comparable, an MCMG calculation was performed with infinite radial extent for the 200-cm-long concrete cylinder. The results were essentially identical to those with the 100-cm radius.

To further complete the picture (but not belabor the point), ONETRAN was also used with a 30-group ENDF/B-V multigroup cross-section set. The transmitted leakage was virtually identical with the ENDF/B-IV results from ONETRAN and MCMG. Finally, MCNP calculations were made with modified 240-group discrete-reaction cross sections based on ENDF/B-V. The cross sections for both silicon and oxygen were modified to accurately represent the large window in the total cross section for each nuclide, at 0.145 MeV for silicon and 2.35 MeV for oxygen. The result was the same as with the regular discrete cross sections in which the windows are averaged out. This indicates the difference between continuous energy and multigroup treatments is due to a self-shielding effect.

Another potential method to improve the results at the exit surface is to surround the surface with a DXTRAN sphere. DXTRAN, however, is generally only useful in situations where it is difficult to get tracks by a random walk to a particular place in the geometry in order to make a tally. This is not the case here since by geometric splitting an abundance of tracks gets to the surface tallies. In this case DXTRAN makes the problem more inefficient by adding additional arithmetic complexity for the computer to handle. However, if one is interested in calculating the flux at a point in the center of the exit surface, relatively few tracks are in the vicinity of any given point on the surface. A surface tally therefore is useless, and a point detector is required. Placing a DXTRAN sphere around a detector can improve the efficiency of a detector calculation significantly.

Table 5. Comparison of Partial Leakage as a Function of Method and Thickness

Surface	J^+MCNP	J^+DRXS	J^+MCMG	MCNP/DRXS	MCNP/MCMG
15 cm	7.44E-2 (.68%)	7.38E-2 (.62%)	7.35E-2 (.46%)	1.01	1.01
30	2.66E-2 (6.6%)	2.58E-2 (1.0%)	2.48E-2 (.74%)	1.03	1.07
45	8.07E-3 (1.5%)	7.65E-3 (1.4%)	7.00E-3 (1.0%)	1.05	1.15
60	2.26E-3 (1.9%)	2.14E-3 (1.8%)	1.79E-3 (1.3%)	1.06	1.26
75	6.14E-4 (2.4%)	5.69E-4 (2.2%)	4.40E-4 (1.7%)	1.08	1.40
90	1.61E-4 (2.9%)	1.48E-4 (2.7%)	1.06E-4 (2.1%)	1.09	1.52
105	4.25E-5 (3.5%)	3.81E-5 3.2%)	2.55E-5 (2.5%)	1.12	1.67
120	1.14E-5 (4.1%)	9.62E-6 (3.7%)	5.89E-6 (3.0%)	1.19	1.94
135	3.09E-6 (4.7%)	2.41E-6 (4.4%)	1.40E-6 (3.4%)	1.28	2.21
150	7.99E-7 (5.3%)	6.18E-7 (5.0%	3.31E-7 (3.9%)	1.29	2.41
165	2.13E-7 (6.0%)	1.59E-7 (5.7%)	7.77E-8 (4.4%)	1.34	2.74
180	5.63E-8 (6.8%)	3.91E-8 (6.1%)	1.81E-8 (4.9%)	1.44	3.11
200	8.20E-9 (7.9%)	5.08E-9 (6.8%)	2.17E-9 (5.6%)	1.61	3.78

20-cm-Radius Problem

This problem is identical to the 100-cm-radius problem in every aspect except for the radius. The smaller radius now makes the transverse and backscattered leakages almost identical, $3.84 \times 10^{-2} \pm 0.4\%$. This problem

runs only slightly less efficiently than the 100-cm-radius problem. The reason is that although it is harder to get particles through the cylinder, less time is spent on particles wandering around radially. They are killed by escaping.

This problem was done in only two modes: splitting with MCNP and MCNP with a combination of the weight window and exponential transformation. The exponential transformation by itself on this problem performs very poorly. The importances for splitting were set using the same technique as before, and another (but different) combination of two-for-one and four-for-one splitting resulted. The importance in the last cell was 21233664 as compared to 4194304 for the 100-cm-radius problem. For the case of splitting, the transmitted leakage is $7.50 \times 10^{-10} \pm 5\%$ with 6.0 as a figure of merit. The weight window and transformation (biasing parameter is again 0.7) result is $8.17 \times 10^{-10} \pm 4.9\%$ with 21.5 as a figure of merit.

From the calculation with splitting, the transmitted neutron dose is $2.74 \times 10^{-17} \pm 7.0\%$ mrem/per neutron, and the transmitted flux is $8.06 \times 10^{-13} \pm 6.9\%$ neutron/cm^2.

DXTRAN is also inappropriate for this case as it was for the 100-cm-radius case; the figure of merit is reduced by its use.

BENT-PIPE PROBLEM

This problem is also divided into two parts, both of which are much less demanding than the previous 200-cm-concrete problem. In both cases a 20-cm-radius pipe that is 240-cm long along the axis has a 90° bend in the center and is jacketed concentrically by a 20-cm-thick region of ordinary Portland concrete. In the first case, the pipe is filled with liquid sodium, and in the second case the pipe is void. The geometry is shown in Figure 2. With the sodium, the attenuation from one end to the other is about 10^6 and with the void about 10^3.

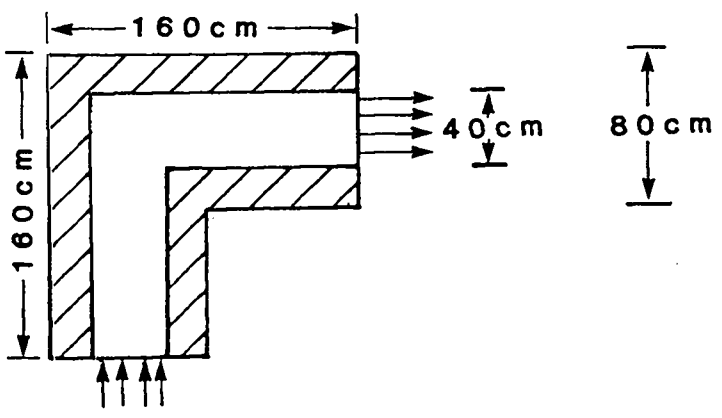

Figure 2. Bent Pipe Jacketed by Concrete.

The source for both cases is the same. It is an area source incident on one end of the pipe (but not including the jacket) with the energy and angular distribution given by

$$S(E,\mu) = \frac{\text{const.}}{E} \qquad \text{(1/E spectrum)} \tag{8}$$

$$= 0 \text{ otherwise} ,$$

where $\mu = +1$ is the cosine of the coaxial direction at the entrance plane. The procedure used to sample this distribution is given in the Appendix at the end of this paper. Constraints on the source are $8.32 \text{ eV} < E < 184 \text{ keV}$ and $0.8 < \mu < 1$.

The tally used to compare the various methods is the leakage transmitted out the opposite end of the pipe (pipe only and not including the jacket) within the direction $0.8 < \mu < 1.0$ where $\mu = +1$ is the cosine of the coaxial direction at the exit plane. Results of other tallies will be reported, however. The energy cutoff in all cases is 8.32 eV.

Sodium-Pipe Problem

The sodium density used is 0.705 g/cm^3 which is appropriate for sodium temperatures of approximately 1000°C. This problem is representative of design features in fast breeder coolant loops and possibly in fusion reactor coolant loops.

With only survival-biasing and a weight-cutoff game, in two minutes of computer time, no tallies were made. In fact, out of 33878 source neutrons, only nine had made it around the 90° bend. No particle got within 40 cm of the pipe exit.

In this problem, the mean free path averaged over collisions for sodium is about 16 cm and about 2 cm in the concrete. Therefore, plane splitting surfaces were placed across the axis of the pipe at 20-cm intervals. A 45° plane was also added where the two legs of the pipe intersect. Radial splitting was used in this problem by adding two concentric cylinders within the concrete jacket to be used as splitting surfaces. The first cylindrical splitting surface was placed 2 cm inside the concrete jacket, and the second was placed outward in the radial direction another 2 cm.

To set the importances, two runs of half a minute each were made to level the track population in the pipe between the source plane and the tally plane. Relative to the corresponding axial importance in the pipe, the radial importances were decreased by a factor of two for each of the first two sleeves and then a factor of four for the outer sleeve. To show that this elaborate radial setup is really not necessary, another run was made with only one radial-splitting surface in the middle of the concrete jacket. The importances of the inner radial cells were reduced by

a factor of two and by another factor of four for the outer radial cells. The figure of merit was 62 with the two concentric splitting surfaces and 58 with only one in the center of the jacket. The two surfaces are more effective in killing outward-bound tracks and maximizing backscattered tracks, but the extra cells and surfaces required more computation time.

In applying the weight window to the sodium pipe, the lower weight bound was derived from the set of importances used in the run with splitting. The lower bound was taken to be $3/I_i$, where I_i is the importance for cell i. The factor three was chosen so that the source particles would start within the weight window. The upper weight bound was taken to be five times the lower weight bound based on previous with the weight window, it was used with the biasing parameter p set to 0.4 in one case and to 0.7 in another.

A multigroup run was made with MCMG using geometry splitting with different axial-splitting planes and with one concentric splitting surface midway between the inner and outer surface of the concrete jacket.

Results of the above cases are summarized in Table 6.

Table 6. Results of Bent Sodium Pipe

Method	Transmitted Leakage ($.8 < \mu < 1$)	% Error	FOM	Computer Minutes
MCNP, splitting	5.83×10^{-7}	4.1	62	9.6
MCNP, weight window	6.38×10^{-7}	6.4	54	4.6
MCNP, weight window, expo. trans.(.4)	5.70×10^{-7}	5.7	67	4.6
MCNP weight window, expo. trans.(.7)	5.93×10^{-7}	6.3	55	4.6
MCMG, splitting	5.19×10^{-7}	5.0	46	8.7
MCNP, splitting, DXTRAN	5.92×10^{-7}	9.9	22	4.6

DXTRAN in conjunction with geometry splitting was tried for a couple of runs with MCNP. The DXTRAN sphere was placed around the sodium at the exit tally plane. A game was played with DXTRAN such that all contributions to the DXTRAN sphere were accepted within four mean free paths, and a Russian roulette game was played with contributions beyond four (a short run indicated about 90% of the contributions were being made within four mean free paths). In one case DXTRAN was tried with the setup with axial-splitting surfaces every 20 cm and with two concentric-splitting

surfaces in the concrete jacket; the figure of merit dropped from 62 to 22. Secondly, DXTRAN was tried with a very simple setup using one axial-splitting surface (four-for-one) at the 45° intersection of the cylinders and a second splitting surface (one-for-two) at the sodium-concrete interface; 0.7 was the figure of merit.

Results other than the transmitted leakage may be of interest. Using MCNP with geometry splitting, 56.5% of the starting weight was lost to energy cutoff, 0.8% to escape through the curved jacket, 0.9% to capture, and 41.2% to backscatter from the source plane. The transmitted leakage out of the sodium was $3.11 \times 10^{-7} \pm 4.3\%$ between 37° and 90° relative to the axis of the pipe at the exit and $5.83 \times 10^{-7} \pm 4.1\%$ between 0° and 37°. The leakage transmitted through the exit plane bounding the concrete jacket (an annular disk excluding the sodium in the center) was $6.27 \times 10^{-8} \pm 7.5\%$ between 37° and 90° and $5.05 \times 10^{-8} \pm 8.3\%$ between 0° and 37°. The neutron dose transmitted through the sodium exit plane was $1.28 \times 10^{-15} \pm 4.4\%$ mrem per neutron, and the dose transmitted through only the concrete at the exit plane was $6.39 \times 10^{-17} \pm 8.6\%$ mrem per neutron. The flux transmitted through the sodium exit plane was $1.01 \times 10^{-9} \pm 4.1\%$ neutrons/cm^2 and $5.02 \times 10^{-11} \pm 7.3\%$ neutrons/cm^2 through the concrete exit plane.

Void-Pipe Problem

This problem is identical to the sodium-pipe problem except that the sodium is replaced by a void. Two surprises came from this problem: (1) intuition led to preliminary problems with geometry splitting, and (2) DXTRAN performed very impressively.

Trying this problem without any variance-reduction techniques, in two minutes of computer time 31448 neutrons started but only 358 got past the 90° bend, and 20 actually got to the exit tally plane.

The splitting surfaces were very similar to the sodium-pipe setup: axial planes every 20 cm and two interior concentric cylinders (one 4 cm into the concrete jacket from the void and the other another 4 cm into the jacket). The final axial importance before the exit was 4096 where it was 2519424 with the sodium. The attenuation from the source to the exit is on the order of 10^3.

Initially the radial importances were set as with the sodium: relative to a given axial cell in the void, the first radial cell had an importance a factor of two less, the middle radial cell importance another factor of two less, and the outer radial cell a factor of four less than the middle cell. This setup led to a figure of merit of 16 which was surprising since the attentuation is three orders of magnitude less than with sodium where the figure of merit was 62.

Looking at the MCNP summary information, it was noted that each neutron created about 7 tracks, and each neutron had about 6.6 collisions. This says that on the average every time a track had a collision, it was

split. This was the clue to the problem: the importance of the inner sleeve of the concrete jacket was a factor of two less than the adjacent void region which meant that a track entering the concrete from the void underwent Russian roulette with 50% survival. If the track backscattered into the void, it was split two-for-one but then immediately went to the other side of the void where Russian roulette was played again, etc. Obviously this is very inefficient.

The next step was to set the importance of the inner sleeve equal to the importance of the adjacent void. The middle-sleeve importance was then reduced by a factor of two relative to the inner sleeve, and the outer-sleeve importance was reduced by a factor of four relative to the middle sleeve.

Playing other splitting games such as changing the thickness of the concrete sleeves and reducing the number of radial sleeves from three to two had relatively little effect.

The weight window by itself was used successfully in the problem; the exponential transformation is not applicable. The bounds of the windows were set based on experience and by experimenting with a couple of short runs and watching the behavior of the sample variance.

MCMG was used with geometry splitting incorporating one concentric splitting surface in the center of the concrete jacket. Furthermore, two scattering kernels were tried: (1) with a continuous-scattering angle and (2) with the MORSE discrete-scattering angle.

Results of these runs are summarized in Table 7.

Table 7. Results of Bent-Void Pipe

Method	Transmitted Leakage ($.8 < \mu < 1$)	% Error	FOM	Computer Minutes
MCNP, splitting	1.08×10^{-3}	5.6	33	9.6
MCNP, weight window	1.10×10^{-3}	4.2	53	10.7
MCMG, splitting, cont. angle	1.11×10^{-3}	3.7	60	12.2
MCMG, splitting, discrete angle	1.07×10^{-3}	3.8	57	12.1

The MCNP-with-splitting figure of merit is less than the others by about a factor of two and less than the sodium-pipe figure of merit also by

a factor of two. The reason for both of these observations is unclear at this point. It can be argued that the void pipe should take longer than the sodium pipe because with the void all scores at the tally come from time-consuming backscattering. With the sodium, a large number of tracks can get to the tally plane without having to backscatter.

DXTRAN with MCNP was tried on this problem in four cases: (1) with the above splitting setup that gave the 33 figure of merit, (2) with the same geometrical setup (all the cells and surfaces set up for splitting) but with importances set to unity, (3) no splitting and all internal cells and surfaces removed that were required for the earlier splitting, and (4) all the extra cells and surfaces still removed but split two-for-one axially where the two legs of the geometry intersect at 45° and reduce the importance of the adjacent concrete jacket by a factor of two relative to the void. The impressive results are shown in Table 8. The weight window was not used for any of these calculations, and there is a potential for further DXTRAN improvements by using it. All runs were for 4.6 minutes of computer time. Russian roulette was played for all contributions to the DXTRAN sphere beyond four mean free paths. In all cases the radius of the outer sphere was 30 cm, and the radius of the inner sphere was 20 cm.

Table 8. DXTRAN Results

Case	Transmitted Leakage ($.8 < \mu < 1$)	% Error	FOM
1 splitting, complex geometry	1.07×10^{-3}	3.8	148
2 no splitting, complex geometry	1.06×10^{-3}	4.0	134
3 no splitting, simple geometry	1.08×10^{-3}	3.3	195
4 mild splitting, simple geometry	1.04×10^{-3}	3.0	243

Some conclusions may be drawn from these DXTRAN calculations. The improvement from case 2 to case 3 points out the obvious: more cells and surfaces require more arithmetic by the computer; they don't come free. Comparing case 1 and case 2 suggests that when you are already doing a pretty good job by one other technique, an additional technique adds little more and may even hurt (this was observed in the other problems). Comparing cases 3 and 4 suggests that there is usually profit in adding a little obvious help to the random walk. Cases 1 and 4 suggest that a very complex, elaborate setup may be overkill; not only does it take a person longer to set up and debug a complicated geometry, it takes the computer a long time to get through it too.

Other results associated with this bent-void pipe include about 1% of the starting weight lost to escape through the curved jacket, 8% lost to backscatter, about 92% lost to energy cutoff, and 0.4% lost to capture. The leakage transmitted from the void at the exit plane between 37° and 90° is $1.65 \times 10^{-4} \pm 5.7\%$, the leakage transmitted from the concrete at the exit plane between 0° and 37° is $7.67 \times 10^{-5} \pm 12\%$ and $5.46 \times 10^{-5} \pm 7.7\%$ between 37° and 90°. The neutron dose through the void at the exit is $1.65 \times 10^{-12} \pm 5.8\%$ mrem per neutron and $6.64 \times 10^{-14} \pm 9.0\%$ through the concrete. The flux through the void at the exit is $1.16 \times 10^{-6} \pm 4.7\%$ neutrons/cm^2 and $5.25 \times 10^{-8} \pm 8.4\%$ neutrons/cm^2 through the concrete.

CONCLUSIONS

It is virtually impossible to be able to say when to use one variance-reduction technique or another. One needs to have many techniques at his disposal. Furthermore, it is also virtually impossible to be able to prescribe how to use a particular technique. Experience in these matters has no substitute.

Despite the above disclaimer, we will attempt some general conclusions:

It appears the weight-window concept has merit when used in conjunction with other techniques that produce a large weight dispersion. It keeps from wasting time on low-weighted particles and keeps a tally and its variance from being overpowered by a few large-weighted scores. However, we at Los Alamos have not had enough experience with this tool to put it into MCNP permanently. We know relatively little about how to set the bounds of the window - especially if energy dependence is required.

The exponential transformation has very limited use by itself. It should not be used alone but in conjunction with something like the weight window. The performance and especially the reliability of the transformation are sensitive to the biasing parameter which, in our opinion, makes this technique dangerous to use except for the experienced Monte Carlo practitioner. We sometimes refer to the exponential transformation as the "dial-an-answer" technique, because the result of a calculation frequently appears to be a function of the biasing parameter.

Geometry splitting with Russian roulette is our most frequently-used technique. Although other schemes may buy more in particular situations, geometry splitting will virtually always give good returns. Furthermore, it is easy to understand and reliable. An important aspect that is apparent from the calculations in this paper is that performance is fairly insensitive within a broad range to how the splitting is implemented (two-for-one, four-for-one, where the surfaces are located, etc.)

Furthermore, it is not just enough to look at a figure of merit and a final sample error. You must also look at the sample mean and its error at

frequent intervals to make sure they have settled down and converged on a reliable result. In other words, look at the variance of the variance. For example, after a relatively few histories, a point-detector flux may have an indicated error of 10% but be in actual error by several factors. After a few more histories, both the flux and its error could be perturbed significantly. This procedure was not emphasized earlier in the paper, but it was used. It is simply wise practice - because it may give the only clue of an unreliable result.

Group X-6 is experimenting with analytically calculating the variance of the variance (or error of the error) and most of the MCNP calculations for this paper were done with a modification to MCNP for this purpose.[11] We recognize that there is very little quantitative information in the fourth moment, but qualitatively it appears that whenever the error of the error is of the same order as the error (both about 5 or 10%, for example) then the sample mean is reliable. But if the error is about 10% and the error of the error is 60%, the mean is unreliable.

One valid rule of thumb is to always make a few short, experimental runs to get a feel for the problem and to see the effect for different techniques and parameters. The code you are using should automatically provide you with enough basic information to allow you to evaluate and understand the run and its attributes. It has been our observation that the more experience a person has, the more reliance is put on preliminary runs. The less experience a person has, the more likely a job will be set up as quickly as possible, a long run attempted, and whatever comes out believed.

Finally, this paper has probably generated more questions than it has answered - especially in the area of multigroup calculations. Also, as applications become increasingly more complicated, there are other important and interesting topics such as the effect of representing a complex three-dimensional geometry by a lower-dimensional model. We look forward to addressing these and other questions in the future.

Acknowledgment

We wish to acknowledge P.D. Soran of X-6 for the ONETRAN calculation using ENDF/B-V data and for modifying the silicon and oxygen data in the discrete-reaction cross-section set.

REFERENCES

1. "Neutron and Gamma-Ray Flux-to-Dose Rate Factors," ANSI/ANS-6.1.1-1977 (N666), American Nuclear Standards Neutron and Gamma-Ray Flux-to-Dose-Rate Factors, Am. Nuc. Soc. (Illinois, 1977).

2. LASL Group X-6, "MCNP - A General Monte Carlo Code for Neutron and Photon Transport," LA-7396-M, Revised (November, 1979).

3. O. L. Deutsch, "MCMG User's Guide," Internal X-6 Document (March, 1979).

4. L. L. Carter and C. A. Forest, "Transfer Matrix Treatments for Multigroup Monte Carlo Calculations - The Elimination of Ray Effects," Nuclear Science and Engineering, 59, 27 (1976).

5. N. M. Schaeffer, Editor, "Reactor Shielding for Nuclear Engineers," Published by U.S. A.E.C. Office of Information Services, p.451 (1973).

6. "The Analysis and Design of Concrete Radiation Shielding for Nuclear Power Plants," ANSI/ANS-6.4-1977 (N403), American Nuclear Standards Guidelines on the Nuclear Analysis and Design of Concrete Radiation Shielding for Nuclear Power Plants, Am. Nuc. Soc. (Illinois, 1977).

7. G. P. Estes and J. S. Hendricks, "Integral Testing of Some ENDF/B-V Cross Sections," Transactions of the ANS, 33, 679 (November, 1979).

8. R. E. MacFarlane, "Energy Balance of ENDF/B-V," Transactions of the ANS, 33, 681 (November, 1979).

9. R. J. Barrett and R. E. MacFarlane, "Coupled Neutron and Photon Cross Sections for Transport Calculations," LA-7808-MS (April, 1979).

10. T. R. Hill, "ONETRAN, A Discrete Ordinates Finite Element Code for the Solution of the One-Dimensional Multigroup Transport Equation," LA-5990-MS (June 1975).

11. G.P. Estes and E.D. Cashwell, "MCNP Variance Error Estimator," X-6 Activity Report, LA-8232-PR, p. 19 (July-December, 1979).

Appendix

1. Fission-Spectrum Groups for MCMG

The source fraction per group, S_g, is determined from

$$S_g = \int_{E_{g+1}}^{E_g} \left(\frac{2}{\sqrt{\pi}T}\right)\sqrt{\frac{E}{T}}\, e^{-E/T}\, dE, \quad T = 1.30 \text{ MeV} \quad .$$

Group	Lower Bound, MeV	S_g
1	15.0	3.0380E-5
2	13.5	7.8639E-5
3	12.0	2.3568E-4
4	10.0	1.1626E-3
5	7.79	5.9203E-3
6	6.07	1.7678E-2
7	3.68	1.0418E-1
8	2.865	9.1383E-2
9	2.232	1.0877E-1
10	1.738	1.1525E-1
11	1.353	1.1097E-1
12	0.823	1.8153E-1
13	0.50	1.1963E-1
14	0.303	6.9450E-2
15	0.184	3.6918E-2
16	0.0676	2.8169E-2
17	0.0248	6.6880E-3
18	0.00912	1.5188E-3
		0.99955

2. Sample Energy E from Fission Spectrum

$$f(E) = \frac{2}{\sqrt{\pi}\,T}\sqrt{\frac{E}{T}}\, e^{-E/T}$$

$$T = 1.30 \text{ MeV}$$
$$\bar{E} = 3T/2 = 1.95 \text{ MeV} \quad .$$

Let ξ be a random number (0,1),

$$a = (-\ell n\ \xi_o)\cos^2\left(\frac{\pi}{2}\,\xi_1\right) \text{ and}$$
$$E = T(-\ell n\ \xi_3 + a) \quad .$$

3. Sample 1/E Energy Distribution, Angular Distribution, and Spatial Distribution

Let ξ be a random number (0,1),

(a) Energy: $f(E) = (.10)/E \qquad 8.32 \text{ eV} < E < 184 \text{ keV}$

$$E = 0.184e^{-10\xi}$$

(b) Angular: $f(\mu) = \text{const.} \qquad 0.8 < \mu < 1$

$$= 0 \qquad \text{otherwise}$$

$$\mu = 0.8 + 0.2\xi$$

$\mu = +1$ is along y-axis

The direction cosines (u,v,w) = (0,1,0) must be rotated through the polar angle $\cos^{-1}\mu$ and through an azimuthal angle sampled uniformly from $(0,2\pi)$.

(c) Spatial: $y = 0$

$$x^2 + z^2 < 20^2 \quad .$$

☆ U.S. Government Printing Office: 1980 — 677 — 115/84

Printed in the United States of America. Available from
National Technical Information Service
US Department of Commerce
5285 Port Royal Road
Springfield, VA 22161

Microfiche $3.00

001-025	4.00	126-150	7.25	251-275	10.75	376-400	13.00	501-525	15.25
026-050	4.50	151-175	8.00	276-300	11.00	401-425	13.25	526-550	15.50
051-075	5.25	176-200	9.00	301-325	11.75	426-450	14.00	551-575	16.25
076-100	6.00	201-225	9.25	326-350	12.00	451-475	14.50	576-600	16.50
101-125	6.50	226-250	9.50	351-375	12.50	476-500	15.00	601-up	

Note: Add $2.50 for each additional 100-page increment from 601 pages up.